Metabolic Characterization of HiPSC-CMs derived from a Hypertrophic Cardiomyopathy Patient Harboring the MYH7 p.R403L Variant
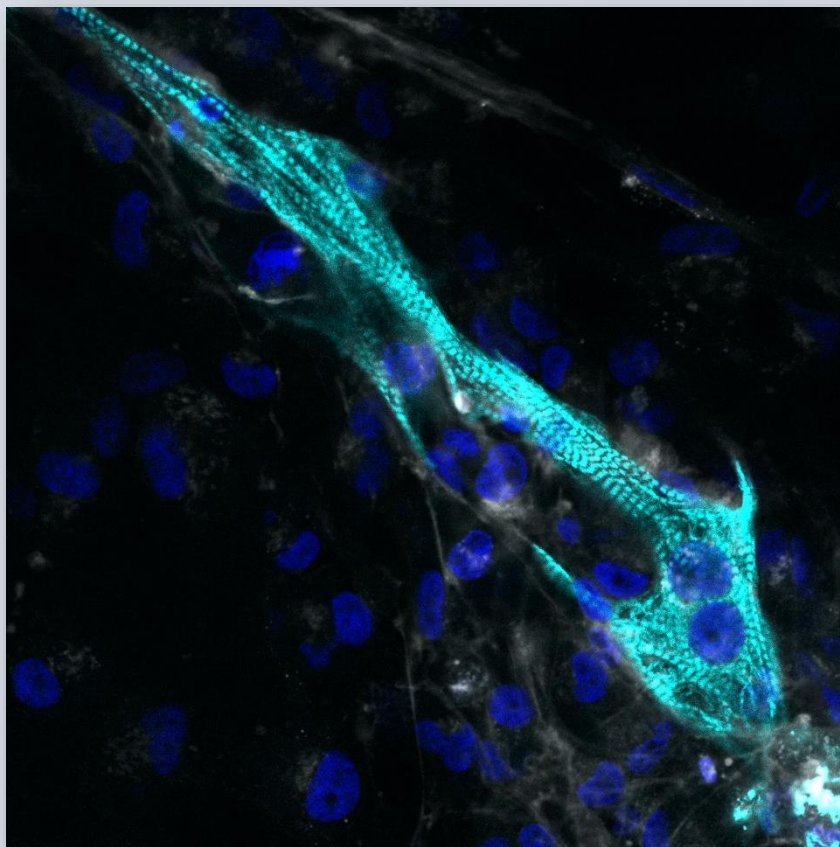
4th of November, 2022
Daniëlle Ammerlaan, BSc
Major Internship report, master Biology of Disease

Cover sheet figure description: Representative immunofluorescence image of an untreated isogenic control cell line stained for the β-myosin heavy chain (MYH7) protein. The image shows heterogeneous MYH7 expression in control cells, thereby highlighting the importance of routine sequencing of human induced pluripotent stem cell-derived cardiomyocytes isogenic control cell lines.

Major internship report, master Biology of Disease, Utrecht University

Daily supervisor: Jiayi Pei, PhD; Examiner: Magdalena Harakalova, MD, PhD; Second examiner: Frank van Steenbeek, PhD.

Department of Cardiology and Regenerative Medicine

Abstract

Hypertrophic cardiomyopathy (HCM) is a severe hypercontractile disorder of the heart affecting 1 in 500 individuals. It is often caused by variants in sarcomere proteins, including the β-myosin heavy chain (MYH7), leading to abnormalities in calcium handling and cellular metabolism. Although the pathogenic variants in *MYH7* are linked to mitochondrial dysfunction, the exact mechanism in HCM remains unknown. In this study, we first metabolically matured human induced pluripotent stem cell-derived cardiomyocytes (hiPSC-CMs) derived from an HCM patient resembling the HCM phenotype. Hereafter, we functionally characterized our model by examining contractile function and mitochondrial respiration. Additionally, we treated the cells with metabolic inhibitors (oligomycin, carbonyl cyanide-4 (trifluoromethoxy) phenylhydrazone, and rotenone/antimycin A) and enhancers (fenofibrate and bezafibrate) and evaluated the metabolic changes using seahorse and immunofluorescent imaging, respectively. In our diseased cell lines, we observed prolonged cardiac contraction, decreased fatty acid oxidation, and minor response upon metabolic inhibition. By re-activating the metabolic activities with fenofibrate, proliferator-activated receptor alpha (PPARA) levels were boosted while hydroxyacyl-CoA dehydrogenase trifunctional multienzyme complex subunit alpha (HADHA) levels remained unchanged. Immunofluorescent staining of sarcomeres using alpha actinin (ACTN2) and MYH7 antibodies revealed sarcomere disarray in diseased cells and recurrence of the variant in one of the isogenic control cell lines. Taken together, our study shows aberrant contractile function, impaired myocardial energy metabolism, and sarcomere disarray in a hiPSC-CMs model carrying the MYH7_R403L variant. Future research should include routine sequencing of hiPSC-CMs lines and improve maturation strategies to model HCM *in vitro*. Additionally, the time point of fibrate administration during pre-clinical *in vitro* studies in HCM should be further optimized.

Keywords: HCM • MYH7 • Lipid metabolism • Contractility • HiPSC-CMs maturation

Laymen's summary

Hypertrophic cardiomyopathy (HCM) is a serious disease in which the heart muscle is thickened. It is generally caused by genetic mutations and takes the lives of 1 in 500 people. Normally, the heart pumps blood through the body due to a structure that is able to contract and relax, called a sarcomere. This structure needs energy generated from fuels, like fats and sugars, to work efficiently. However, in HCM patients, the heart burns less fats than it is supposed to do. This leads to problems with the generation of energy during contraction and relaxation of the heart. In our study, we grew heart cells in a dish and tried to mimic the diseased state. We also grew healthy control cells and gave both cell types an ideal combination of nutrients to make them mature. Afterward, we recorded the diseased and healthy control cells that were beating and performed a test that measured the oxygen consumption. We added drugs that inhibit energy production to a certain extent and found that the diseased cells were barely responding, indicating that fat burning is incredibly low. We also added another drug, called fibrates, that stimulated the heart cells to produce more energy from the burning of fats. Proteins of interest were stained with a fluorescence color making it possible to determine their levels with a fluorescence detecting microscope. We found that our cells respond to one specific fibrate that increases levels of proteins that are involved in the fat burning process. Although further research is required, this discovery offers opportunities for future lifestyle implementations and treatments for both people at risk and HCM patients.

Graphical abstract
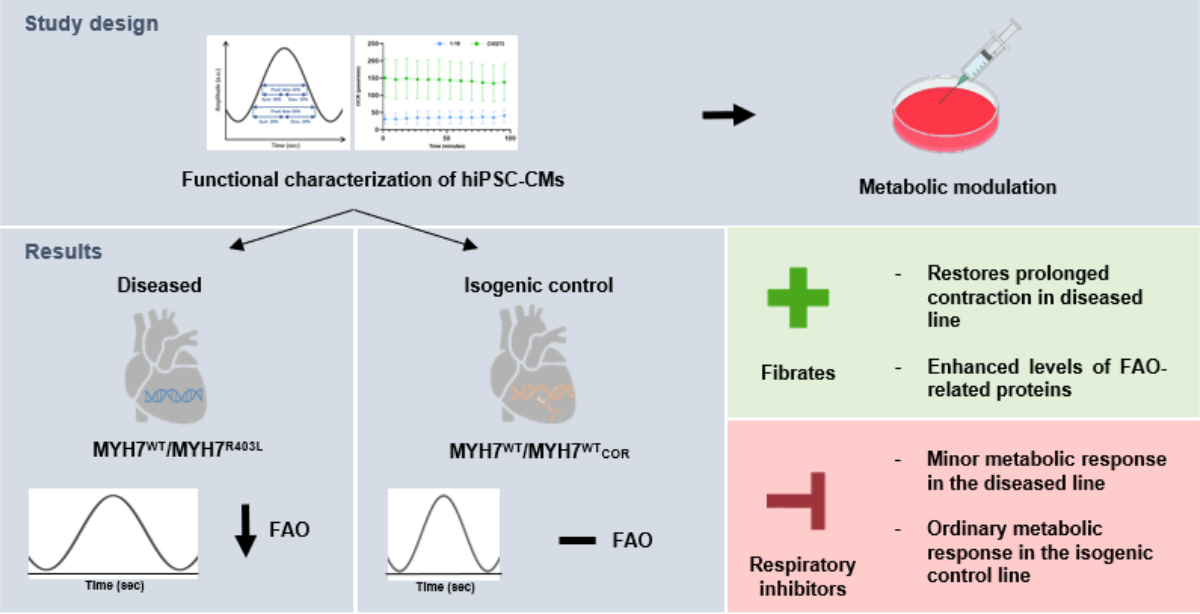
Metabolic characterization and treatment of hiPSC-CMs. *In vitro* matured diseased and CRISPR/Cas9 corrected isogenic control hiPSC-CMs were first functionally characterized using contractile function assays and seahorse assays. Here, we observed a prolonged contraction time and decreased FAO in the diseased line compared to the isogenic control line. Next, metabolic stimulators (fibrates) or inhibitors (oligomycin, FCCP, R/A) were added to both lines separately. Upon fibrate treatment, the diseased line showed an improved contraction time and increased the levels of proteins involved in mitochondrial FAO. Addition of respiratory inhibitors during the mitochondrial stress test provoked a minor response in the diseased cells as compared to the isogenic control lines. In conclusion, this study revealed that fibrates beneficially affect overall contraction time and FAO-related protein levels. However, further research into the timing of fibrate administration in matured *in vitro* models remains crucial. hiPSC-CMs = human induced pluripotent stem cell-derived cardiomyocytes, FAO = fatty acid oxidation, MYH7 = myosin heavy chain, FCCP = carbonyl cyanide-4 (trifluoromethoxy) phenylhydrazone, R/A = rotenone/antimycin A.

Abbreviations

ACTN2	Alpha actinin
BSA	Bovine serum albumin
CD36	Cluster of differentiation 36
DMEM	Dulbecco's modified eagle medium
ECAR	Extra cellular acidification rate
FAO	Fatty acid oxidation
FCCP	Carbonyl cyanide-4 (trifluoromethoxy) phenylhydrazone
FDA	Food and drug administration
FFAs	Free fatty acids
HADHA	Hydroxyacyl-CoA dehydrogenase trifunctional multienzyme complex subunit alpha
HCM	Hypertrophic cardiomyopathy
HiPSC-CMs	Human induced pluripotent stem cell-derived cardiomyocytes
HPLC	High performance liquid chromatography
IF	Immunofluorescent
KLF15	Krüppel-like factor 15
KO serum	KnockOut serum replacement
MYBPC3	Cardiac myosin binding protein C
MYH7	β-myosin heavy chain
OCR	Oxygen consumption rate
PBS	Phosphate-buffered saline
PDK4	Pyruvate dehydrogenase kinase 4
PPARA	Peroxisome proliferator-activated receptor alpha
R/A	Rotenone/Antimycin A
ROI	Region of interest
RPMI	Roswell park memorial institute
TNNT2	Troponin T
WGA	Wheat germ agglutinin

1. Introduction

Hypertrophic cardiomyopathy (HCM) is a genetic disorder affecting 1 in 500 individuals.[1] Characteristics include myocardial thickening, systolic and diastolic dysfunction, sarcomere disassembly, and impaired energy metabolism of the cardiac muscle, which can result in left ventricular outflow tract obstruction, heart failure, and sudden cardiac death.[2,3] Over 1,500 pathogenic variants in sarcomere-associated proteins have been identified, of which β-myosin heavy chain (*MYH7*) and cardiac myosin binding protein C (*MYBPC3*) are responsible for 80% of the HCM cases. The proteins are located in the thick filament of the sarcomere and are encoded by the *MYH7* and *MYBPC3* gene, respectively.[4,5] Common pathogenic variants leading to a HCM phenotype in *MYBPC3* include p.R502W and p.V762D.[6,7] These missense variants are associated with a milder disease course compared to *MYH7* variant carriers. For instance, patients harboring pathogenic variants in the *MYH7* gene present with an increased prevalence of atrial fibrillation and systolic anterior motion of the mitral valve, contributing to a more severe phenotype.[7,8] The p.R403L variant in the *MYH7* gene is considered a hotspot variant and is correlated with a high incidence of sudden deaths and severe cardiac events.[9] In addition to a worse outcome compared to *MYBPC3* variant carriers, incomplete penetrance of the p.R403L variant calls for more research into HCM pathology.[8,10] Thus far, it is known that causal pathogenic variants in the *MYH7* gene induce alterations in calcium handling and activation of signaling pathways, such as mitogen-activated protein kinase. Furthermore, HCM pathogenesis is accompanied by histological alterations, including interstitial fibrosis and myocardial disarray.[6,11] To date, a few effective treatments are available for HCM patients but the main focus has been laid on symptom relief, such as beta-blocker and calcium channel blocker therapy.[12] Recently, a cardiac myosin head inhibitor, mavacamten, has been approved by the food and drug administration (FDA) for the treatment of obstructive HCM patients. By stabilizing the relaxation state of the myosin head, mavacamten is able to improve diastolic function significantly.[13] As obstructive HCM is prevalent in 70% of the HCM patients and does not tackle the entire clinical picture of HCM, research aims for further improvement of HCM pathology.[13,14]

Interestingly, mounting evidence has suggested a clear link between sarcomere variants and mitochondrial dysfunction.[1,15–17] A clinical study performed by Crilley *et al.* showed altered myocardial energetics in both asymptomatic variant carriers and HCM patients, carrying a *MYH7*, *MYBPC3*, or cardiac troponin T (*TNNT2* and *TNNI3*) variant, indicating that metabolic perturbations already occur before the onset of hypertrophy.[1] This was supported by findings demonstrating a shift from fatty acid to glucose metabolism in asymptomatic variant carriers.[15] In advanced HCM, similar metabolic alterations are present. Recent studies using *MYH7* and *MYBPC3* mutated human left ventricular septal myectomy samples from patients with severe HCM reported global cardiometabolic dysregulation.[4,16,18,19] A marked reduction was observed in metabolites of the glycolytic, pentose phosphate pathway, and tricarboxylic acid cycle in HCM samples compared to donor's hearts.[16] Detailed proteome and transcriptome analysis further revealed significant downregulation of mitochondrial lipid metabolism in HCM hearts, which can have detrimental effects as lipids are the preferred energy substrate of the cardiac muscle.[4,16] This includes downregulation of genes involved in the transport and oxidation of long-chain fatty acids, such as cluster of differentiation 36 (CD36) and hydroxyacyl-CoA dehydrogenase trifunctional multienzyme complex subunit alpha (HADHA) respectively.[16] Frequently, these genes are regulated by the nuclear transcription factors peroxisome proliferator-activated receptor alpha (PPARA*)* and krüppel-like factor 15 (KLF15) in the cardiac muscle.[20] As both factors co-operate to stimulate the fatty acid oxidation (FAO), which is downregulated in HCM, and gene set enrichment analysis correlated *PPARA* to the *MYH7* gene, this proposes a potential role of PPARA in HCM pathology.[17,20]

PPARA agonists, such as fenofibrate and bezafibrate, are already applied in clinical trials for metabolic diseases, such as type II diabetes, where it has been shown to improve lipid profiles.[21,22] In cardiomyocyte models, both fenofibrate and bezafibrate treatment were associated with diminished cardiac hypertrophy.[23,24] However, it remains incompletely understood whether fibrate treatment decreases cardiac hypertrophy via its effect on mitochondrial metabolism and PPARA.

Over the past decade, the use of human induced pluripotent stem cell-derived cardiomyocytes (hiPSC-CMs) as a disease model, in particular for genetic cardiomyopathies, has emerged. With the use of patient-specific hiPSC-CMs, the causality of genetic variants in relation to metabolic alterations occurring in HCM can be examined. In addition, hiPSC technology provides the possibility to study disease development chronologically and compensates for the lack of myocardial tissue availability.[25] Despite its promising future as an *in vitro* research model, immaturity of the hiPSC-CMs has been a limitation so far.[26] Features of matured iPSC-CMs include increased oxidative capacity, enhanced use of fatty acids as energy substrates, and sarcomere development.[27] To enhance iPSC-CM maturation, long-term culturing with a newly developed maturation medium, characterized by low glucose and high fatty acid substrate availability, has been shown to be effective.[28,29] Additional maturation strategies include electromechanical stimulation and cultivation on nanopatterned surfaces.[30,31]

In this study, we aimed to characterize the diseased and isogenic control hiPSC-CM lines and examine their metabolic profiles upon treatment with inhibitors and enhancers. We first performed an extensive analysis of the medium components present during the several culturing phases that achieve subsequent hiPSC-CM proliferation and maturation. This detailed overview gives insight into the factors that can influence cardiac metabolism substantially. Next, we characterized the cellular morphology, contractility, myocardial metabolism, and protein levels (ACTN2, MYH7, PPARA, HADHA, CD36, KLF15) of our diseased and isogenic control lines. After functional assessment of the *in vitro* models, we treated the cells with metabolic enhancers and inhibitors. Our findings show a prolonged cardiac contraction and a decreased FAO in the diseased line compared to the isogenic control line. Moreover, metabolic stimulation with the PPARA agonists fenofibrate and bezafibrate showed that the diseased cells respond to fenofibrate treatment as confirmed by the increase in PPARA protein levels. Further research and optimization of the time of fibrate application in pre-clinical models is, however, required for the therapeutic application of these drugs in HCM patients.

2. Materials and Methods

A complete list of the used materials and their catalog numbers can be found in Supplementary file 1.

2.1 Cell culturing

A forearm skin biopsy was taken from a female HCM patient carrying the p.R403L variant in the *MYH7* gene. Informed consent was obtained to perform the biopsy and generate the hiPSC-CMs lines. From the harvested skin fibroblasts, reprogramming towards hiPSCs was performed as described in the paper of Okita *et al.*, after which directed cardiomyocyte differentiation was accomplished by applying the GiAB protocol from Lian *et al.*.[32,33] Two hiPSC-CM clones (CDGEN1-6 and CDGEN1-16) were generated by the group of Dr. Villard, our collaborators from Paris. Using CRISPR/Cas9 editing, the variant was corrected, thereby creating the corresponding isogenic control cell lines CDGEN1-6-24 and CDGEN1-16-40.5 and excluding interpatient variability.[34] The 1-6 and 1-6-24 hiPSC-CM lines were used for the assessment of cardiac contractility and immunofluorescent (IF) staining experiments, whereas the 1-16 and 1-16-40.5 lines, and a wildtype control line, CVI273, were used for the seahorse assay. 1-16-40.5 isogenic controls were used for IF antibody testing. Throughout the cultivation period, cells were maintained in the Panasonic MCO-170AIC CO_2 incubator under the following conditions: 37.5 degrees Celsius and 5.0% CO_2.

2.1.1 Thawing

After thawing of the hiPSC-CM cryovials from the -196 degrees Celsius nitrogen tanks, cells received a thawing medium for 24 hours. This medium is composed of 10% KnockOut serum replacement (KO serum) and 1% RevitaCell supplement that boost the growth and recovery of the cells (Supplementary table 1).

2.1.2 Proliferation phase

After 24 hours on thawing medium, cells were cultured in proliferation medium (96.7% Roswell Park Memorial Institute (RPMI), 2% B27 plus insulin, and 1% penicillin and streptomycin) supplemented with 0.005% CHIR99021 and 0.031% insulin (Supplementary table 1). CHIR99021 greatly enhances cardiomyocyte proliferation by interfering in the Wnt/β-catenin signaling pathway.[35] It inhibits glycogen synthase kinase, thereby preventing the destruction of the β-catenin complex. β-catenin can, in turn, initiate the transcription of genes that promote cell proliferation and insulin sensitivity. Insulin supplementation serves as an extra metabolic stimulator.[35] The medium was refreshed every other day to ensure the cells received enough nutrients for optimal proliferation. Cell growth was monitored using the Olympus CKX41 Inverted Microscope and brightfield images were taken every other day at 4x magnification.

2.1.3 Replating

Once 90% confluency was reached, cells were detached by the incubation with TrypLE select (10x) for 10-15 minutes and replated into a new Matrigel-coated T75 flask, 6 wells plate, or 24 wells plate for further proliferation. The Countess II FL Automated Cell counter was used to equally divide the live cells over the flasks or wells. To ensure full recovery, hiPSC-CMs were first cultured in a replating medium, containing 10% KO serum and 0.1% RevitaCell supplement, for 24 hours before the cultivation using a proliferation medium (Supplementary table 1).

2.1.4 Maturation phase

Metabolic maturation of the hiPSC-CMs was accomplished by providing an optimal set of organic and inorganic compounds that stimulate the cells to shift towards aerobic oxidation. Long-term maturation on maturation medium has been shown to enhance physiological maturation, thereby creating a better *in vitro* disease model.[28] Maturation medium consists of 85% Dulbecco's Modified Eagle Medium

(DMEM) without glucose, 10% maturation master mix, 2% B27 plus insulin, 2% KO serum, and 1% penicillin and streptomycin. An extensive Excel file was created containing all components present over time in the abovementioned culturing media (Supplementary table 1). Herein, it was reported which components are present in each phase, what their working concentration is, and from which sources the component is derived from. A schematic overview of the components is shown in Supplementary file 2 while detailed protocols describing cardiomyocyte differentiation, expansion and maturation are available in Supplementary files 3-6.
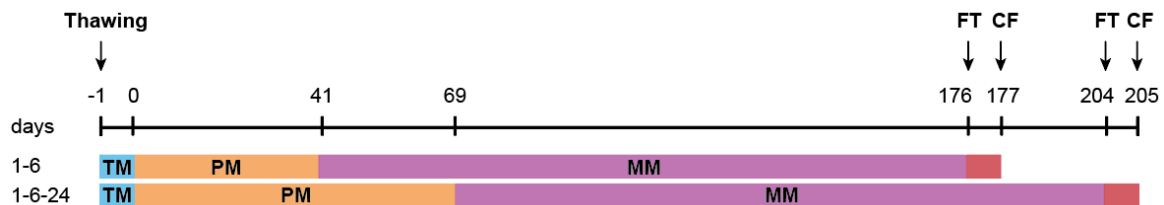
Figure 1: Timeline of the 1-6 and 1-6-24 cell culturing process. After thawing of the 1-6 and 1-6-24 cryovials, the hiPSC-CMs were cultivated for 24 hours on a thawing medium (TM). Hereafter, cells were grown in a proliferation medium (PM) in T25, T75, and 6 wells plates. The isogenic control, 1-6-24, proliferated much slower and was therefore put on a proliferation medium for a longer period. Both the 1-6 and 1-6-24 cell lines were matured for 135 days on a maturation medium (MM). After 134 days of maturation on Matrigel-coated coverslips, the hiPSC-CMs were incubated with either 100 µM fenofibrate or 100 µM bezafibrate for 24 hours. Control hiPSC-CMs were cultured for 135 days in a MM. After the fibrate treatment (FT), cell fixation (CF) with 4% paraformaldehyde was performed. TM: thawing medium, PM: proliferation medium, MM: maturation medium, FT: fibrate treatment, CF: cell fixation.

In this study, the proliferation medium was replaced by a maturation medium for the 1-6 and 1-6-24 cell lines at day 41 and 69 of cultivation, respectively. A slower proliferate rate was observed in the 1-6-24 line as compared to the 1-6 line. To obtain sufficient cells for the planned experiments, 1-6-24 cells were cultured longer in the proliferation medium. Afterward, both the 1-6 and 1-6-24 cell lines were seeded to Matrigel-coated coverslips in a 24 wells plate ($1.8*10^5$ cells/well) and cultured for 135 days in a maturation medium, followed by fixation and staining of the cells (Figure 1).

2.2 Experimental fibrate treatment
At 134 days of maturation, 1-6 and 1-6-24 hiPSC-CMs were treated with the FDA-approved PPARA agonists, namely 100 µM fenofibrate or bezafibrate, for 24 hours. This working concentration was prepared using dimethyl sulfoxide as a solvent and the maturation medium to make a 1,000x dilution from our 100 mM stock. Besides the agonist-supplied maturation medium, the basal maturation medium was included as the control condition. For each well, an end volume of 1 mL was reached. For both the 1-6 and 1-6-24 cell lines, eight coverslips were available. For the experimental conditions, fenofibrate and bezafibrate treatment, three coverslips per line were assigned to each one of them. This way, we could perform three different co-stainings on a specific fibrate-treated coverslip. For the control condition, two coverslips per line were available. Incubation times and concentrations of the fibrates were based on a literature search and inhouse data obtained from *PLN R14del* hiPSC-CMs and isogenic controls suggesting the restoration of impaired mitochondrial metabolism under the same experimental conditions (Supplementary table 2).

2.3 Immunofluorescence staining and imaging
After fibrate treatments, 1-6 and 1-6-24 coverslips were stained with several primary and secondary antibodies following an optimized two-day staining protocol (Supplementary file 7). Briefly, cells were washed once with phosphate-buffered saline (PBS) and fixed by the incubation with 4%

paraformaldehyde for 10 to 15 minutes at room temperature. After 1 hour of blocking with bovine serum albumin (BSA), cells were incubated for 1 hour with wheat germ agglutinin (WGA) in a 1% BSA/PBS solution. After washing with PBS once, overnight incubation with primary antibodies (MYH7, HADHA, ACTN2, PPARA, CD36, KLF15) at 4 degrees Celsius was performed. On the second day of IF staining, cells were washed three times with PBS, followed by the incubation with the secondary antibodies for 1 hour at room temperature. Hereafter, DAPI was added for 10 minutes, coverslips were washed with PBS, mounted, and put on a glass slide. MYH7, HADHA, ACTN2, and PPARA stainings were performed in untreated, fenofibrate-treated, and bezafibrate-treated hiPSC-CMs, whereas CD36 and KLF15 stainings were only executed in the fibrate-treated conditions due to the limited availability of the cells. Dilutions of the antibodies are mentioned in Supplementary file 7.

IF images were made with the Leica SP8-X Confocal Microscope using the Las X software (format: 2,048*2,048, speed: 100). Laser intensities were optimized per staining and remained the same throughout analysis of a specific condition (Supplementary file 8). IF images were made with the 63x magnification objective using Olympus immersion oil IMMOIL-F30CC. IF images were processed using Fiji and CellProfiler 4.2.1. Briefly, the lif file from the LasX program was first imported into Fiji (ImageJ 1.53t) to create hyperstacks of the selected images. Hereafter, each hyperstack was manually saved in tiff format and uploaded to CellProfiler. Detailed information about the CellProfiler pipeline per staining is depicted in Supplementary file 8. In brief, the area and intensity of the stainings were quantified using the 'Measure image area occupied' and 'Measure image intensity' modules. Afterward, the value was divided by the quantified DAPI signal per IF image to normalize the signal to the number of nuclei (Supplementary table 3-5). Outliers were excluded for further analysis using the GraphPad outlier test. As a statistical method, 1-way ANOVA was used to compare the different treatments with the untreated condition within one cell line. 2-way ANOVA with multiple comparisons ('compare each cell mean with the other cell mean in that column') was used to perform statistical analysis of the same treatment between the two cell lines for the ACTN2, MYH7, PPARA, and HADHA stainings (Figure 4). Unpaired student's t-test was applied for the CD36 and KLF15 stainings under default settings (Figure 5). Graphs were made with GraphPad Prism 9.3.0.

Optimization of the primary and secondary antibodies used in this study was performed using +/-30 days matured 1-16-40.5 hiPSC-CMs. Details and results of the test stainings can be found in Supplementary file 9.

2.4 Mitochondrial stress test using Seahorse
To assess aerobic respiration, 1-16, 1-16-40.5 hiPSC-CMs, and CVI273 control cells were seeded to the Matrigel-coated seahorse microplate ($4*10^4$ cells/well) and matured for 35 days, after which they were analyzed using the Agilent Seahorse XF cell mitochondrial stress test. Cells were first washed three times with seahorse XF base medium supplemented with 3 mM D-glucose, 4 mM glutamine, and 2% B27 plus insulin to mimic the metabolic maturation medium. Afterward, 525 µL of the medium was added to each well. Except for nine 1-16 and nine CVI273 control wells, three different mitochondrial inhibitors were loaded to the injection ports of the cell culture microplate wells. The defined working concentration of the inhibitors in the well was 2.5 µM oligomycin, 2 µM carbonyl cyanide-4 (trifluoromethoxy) phenylhydrazone (FCCP), and 2.5 µM rotenone mixed with antimycin A (R/A). The inhibitory compounds were sequentially injected while running the assay. After calibration of the Agilent Seahorse XFe24 extracellular flux analyzer, the plate was placed in the machine and the assay was initiated. Throughout the assay, the oxygen consumption rate (OCR) and extra cellular acidification rate (ECAR) were assessed in the different phases while a temperature of 37 degrees Celsius was maintained. A complete user guide of the mitochondrial stress test is depicted in Supplementary file 10. For data analysis, significant outliers

were excluded using the GraphPad outlier test. 1-way ANOVA with multiple comparisons ('compare the mean of each column with the mean of every other column') was performed to detect differences between the different cell lines upon metabolic inhibition (Figure 6d, 6f). Raw data from Figure 6 can be found in Supplementary table 6.

2.5 Contractility assay of individual beating hiPSC-CMs
Directly before and after 24-hour fibrate incubation, brightfield videos of 15-20 seconds were made using the 10x objective lens on the Olympus CKX41 Inverted Microscope. With the Any Video Converter application, all videos were converted to AVI format. After loading the Myocyter v1.2.0039 plugin onto the ImageJ1.52s platform, the macro was run step by step according to the Myocyter manual with minor adjustments.[36] For each brightfield video, we manually selected the region of interest (ROI), followed by an evaluation of those ROIs per video. After the evaluation step, additional steps that the 'Run Macro' option in the Myocyter plugin is offering, were not necessary to quantify the cardiac contractions in the coverslips before and after treatment. A clear protocol describing each step of the quantification of cardiac contractions in ImageJ can be found in Supplementary file 11. Raw data are displayed in Supplementary table 7.

From the ImageJ output, data of one complete cardiac contraction (a peak in the middle of the data plot) was selected per cell to include in the graphs. Again, on each data set, the GraphPad outlier test was performed. On each individual data set, statistical analysis was performed. Data sets before fibrate treatment were compared using the unpaired student's t-test under default settings (Figure 2b-i). After fibrate treatment, 1-way ANOVA was used to compare the different treatments with the untreated condition within one cell line. 2-way ANOVA with multiple comparisons ('compare each cell mean with the other cell mean in that column') was used to perform statistical analysis of the same condition between the two cell lines (Figure 3b-i).

2.6 Quantification of spontaneously beating cardiac 3D clusters
Brightfield images were also made throughout the cultivation process. In the maturation phase, spontaneously developing 3D cardiac clusters were observed in the 1-6 and 1-6-24 cell lines (Figure 7). Areas of the clusters observed during 135 days of maturation were manually selected and quantified using the 'measure' feature in ImageJ 1.52s. Print screens of each drawing surrounding a 3D cardiac cluster are displayed in Supplementary file 12. On each data set, the GraphPad outlier test was performed after which the significant outliers were excluded for further analysis. The contrast of the representative images was adjusted using the auto contrast feature in Adobe Photoshop 2022 (Figure 7a). The raw images are present in Supplementary image 3 and 4. Unpaired student's t-test (Figure 7b, 7e) and two-way ANOVA (Figure 7c, 7f) were performed under default settings when applicable. Simple linear regression was used as a statistical method for the correlation plot (Figure 7d).

Besides, data on Z-sizes in stained and treated 1-6 and 1-6-24 hiPSC-CM lines were manually obtained using the Leica SP8-X Confocal Microscope. Z-stack videos, one of each condition, were made (format: 1,024c*1,024, speed: 400), which allowed us to gain insight into the thickness of the sarcomere structures in the coverslips after long-term maturation (Supplementary videos 1-6). The Z-position of a sarcomere structure was recorded when the sarcomere signal in the *MYH7* channel was completely absent. If the sarcomere did not fit the window, the Z-size was recorded on several spots throughout the cluster, after which the Z-size was averaged and used for further quantification. As a statistical method, 1-way ANOVA was used to compare the different treatments with the untreated condition within one cell line, whereas 2-way ANOVA with multiple comparisons was used to detect differences of the same treatment between the two cell lines (Figure 7h). Raw data from Figure 7 can be found in Supplementary table 8.

3. Results

3.1 Characterization of media composition throughout hiPSC-CMs culturing

As the development of cardiomyocytes can be influenced by culture media, detailed knowledge of the composition of the media is a valuable tool for an experimental design.[28] To characterize the composition of cell culture media, several sources were consulted. The media formulation of the RPMI 1640[37], DMEM medium[38], and non-essential amino acids (NEAA) solution[39] was available on the manufacturer's website. Details about additional components added to the basal medium were mentioned in scientific papers describing the differentiation[33], expansion[40], and maturation procedure[28]. For some components, such as the B27 supplement and the KO serum, information was lacking. The B27 supplement is continuously present throughout the cultivation process and responsible for the long-term viability of the cells. Due to a patent, concentrations of the B27 components are confidential, thus unavailable[41]. However, the Jacob Hanna Lab does provide a B27 supplement protocol that includes concentrations of the different components[42]. For this analysis, the B27 protocol from the Jacob Hanna Lab was used as an estimation. A comparison between the manufacturer's B27 and the Jacob Hanna lab B27 can be found in Supplementary file 13. The composition of the KO serum was available in the paper of Garcia-Gonzalo *et al*.[43] However, concentrations of the components within KO serum were not provided. Therefore, the concentration of a component containing 1% KO serum was defined as 'x' in our overviews while unknown concentration of 0.5% AlbuMax-II is represented with '0.5y' in the table. In addition, the free fatty acids (FFAs) present in AlbuMax-II were not specified. An estimated concentration, based on AlbuMax-I data, was calculated in Section 3.1.2.

Components from the differentiation, proliferation, and maturation medium from the Excel file were visualized in a schematic overview using Adobe Illustrator 2022. The created PDF document displays the components sorted per category and a graph per component shows how the concentration fluctuates throughout the culturing process. The color of the line represents the source of which the component is derived from. The end concentration that the cells receive can be obtained easily by adding the concentration of all lines from one graph together. The Y-axis was scaled for each graph separately to create clear graphs. Concentrations smaller than 0.01 are displayed using scientific notation. The complete PDF document is available in Supplementary file 2.

3.1.1 Huge accessibility of FAO substrates in maturation medium compared to proliferation medium

Using a maturation medium in addition to proliferation medium for the cultivation of hiPSC-CMs is very novel. Therefore, a comparison between the proliferation medium and the maturation medium was made to establish the effects on mitochondrial metabolism. As the 1-6 and 1-6-24 cell lines were treated with PPARA agonists that affect FAO, we first assessed the changes in fatty acid concentration. The fatty acids in the media are derived from the KO serum, B27 supplement, or, the AlbuMax-II component. The B27 supplement is consistent throughout the culturing phases. In contrast, KO serum and AlbuMax-II are only present during the maturation of the hiPSC-CMs. This translates into a huge increase in fatty acid substrate availability once the maturation phase is initiated. In addition, the concentration of L-carnitine hydrochloride, responsible for the transport of long-chain fatty acids into the mitochondrial matrix, is increased in the media of maturing cardiomyocytes.[44] Besides fatty acids, an overall increase in the concentration of other energy substrates and nutrients is observed in the maturation medium compared to the proliferation medium. This includes L-lactate (0 to 10 mM), amino acids (6.55 to (13.38 + 11*x mM)), and inorganic salts (139.05 to 163.24 mM). The vitamin concentrations remains relatively stable over time (1 to (0.91 + x) mM). On the other hand, the glucose supply is decreasing dramatically from 11.11 mM to 3 mM when the switch to a maturation medium is induced (Table 1).

Table 1: Changes in concentration of medium components upon proliferation and maturation of the hiPSC-CM lines. Characterization of the media components over time revealed an overall increase in the energy substrates and nutrients in the maturation phase compared to the proliferation phase.

Energy substrate or nutrient	Concentration present in proliferation medium (mM)	Concentration present in maturation medium (mM)
Free fatty acids	0	25.29 mg/L + x
Triacylglycerides	0	2.78E-02 + x
L-carnitine	0.51	2.00
D-glucose	11.00	3.00
L-lactate	0	10.00
Amino acids	6.55	13.38 + 11*x
Vitamins	1.00	0.91 + x
Inorganic salts	139.05	163.24

3.1.2 Estimated calculation of the FFA concentrations in AlbuMax-II

In the Excel file, it can be appreciated that the maturation medium contains 0.5% AlbuMax-II (Supplementary table 1). Garcia-Gonzalo *et al.* analyzed the lipids present in 1% AlbuMax-II by high-performance liquid chromatography (HPLC, Table 2), but does not specify the FFAs.[43] For our research question, however, it is relevant to know which and how much FFAs are present in the maturation medium as they influence aerobic metabolism. Unfortunately, FFA concentrations in AlbuMax-II are not reported. To approximate the concentration of the FFAs in AlbuMax-II, we used the information from the manufacturer's website on the AlbuMax-I version (Table 3, Column 1).[45] AlbuMax-I, which is a lipid-rich BSA solution as well, has a lower IgG content compared to the AlbuMax-II version.[46] As this extra purification step is the only difference, FFA concentrations in AlbuMax-I are a good estimation for the FFAs present in AlbuMax-II.

Table 2: Lipid components present in AlbuMax-II. High Performance Liquid Chromatography analysis revealed the different lipid species present in 1% AlbuMax-II.[43]

Lipid species	µg/ml in 1% AlbuMAX
Free fatty acids (FFAs)	35.29
Lysophosphatidylcholine (LPC)	11.30
Triacylglycerides (TAGs)	9.79
Phosphatidylcholine (PC)	5.29
Phosphatidic acid (PA)	2.07
Cholesterol (CH)	0.88
Sphingomyelin (SM)	0.80

doi:10.1371/journal.pone.0001384.t002

The following calculation was made to obtain the working concentrations of the FFAs that the 1-6 and 1-6-24 hiPSC-CMs are supplied with. First, the amount of the FFA in mg/g protein, provided by the manufacturer's website, was converted to grams (Table 3, column 2 and 3). If the numbers in column 3 are divided by the molar mass of each FFA, the amount of FA in mol/g protein is obtained. Next, the last column can be used to determine the ratio of the different FFAs.

Next, if you sum all numbers in mol FA/g protein, which equals 100%, the ratios of each FFA can be determined (Table 4). As depicted in Table 2, the total amount of FFAs in 1% AlbuMax-II is 35.29 µg/mL, which equals 35.29 mg/L. In maturation medium, containing 0.5% AlbuMax-II, 17.65 mg/L FFAs is present. In this way, the contribution of each FFA in mg/L can be calculated (Table 4, column 4). The last step is to convert the mg/L into mM by dividing it by the molar mass of the FFA (Table 4, column 5).

Table 3: Calculation of the amount of FA per gram protein in AlbuMax-I. The numbers in mg FFA/g protein were available on the manufacturer's website. Example calculation of alpha-linolenic acid: 0.59 mg FFA per gram protein equals 0.00059 g FFA per gram protein. 0.0059 divided by the molar mass of alpha-linolenic acid, 278.43 = $2.12*10^{-6}$.

FFAs present in AlbuMax-I	mg FFA/g protein	g FFA/ g protein	Molar mass (g/mol)	mol FA/ g protein ($*10^{-6}$)
Alpha-linolenic acid	0.59	0.00059	278.43	2.12
Linoleic acid	0.65	0.00065	280.45	2.32
Oleic acid	2.12	0.00212	282.46	7.51
Stearic acid	2.09	0.00209	284.48	7.35
Palmitic acid	1.90	0.00190	256.42	7.41

Table 4: Calculation of the FFA ratios and working concentration in mM. From Table 3, we obtained the numbers in the first column. The sum of these numbers equals 100%. In this way, the ratio of each FFA can be determined. As 0.5% AlbuMax contains 17.65 mg/L FFAs, you can calculate the contribution of each FFA with the obtained percentage. Example calculation of alpha-linoleic acid: $(2.12*10^{-6})/(26.71*10^{-6})*100\%$ = 7.94%. 7.94% of 17.65 mg/L = 1.40 mg/L. 1.40/278.43 (molar mass) = $5.03*10^{-3}$ mM. N/A = not applicable

FFAs present in AlbuMax-I	mol FA/ g protein ($*10^{-6}$)	% of total	Contribution in mg/L	Amount of FFA in mM ($*10^{-3}$)
Alpha-linolenic acid	2.12	**7.94**	1.40	**5.03**
Linoleic acid	2.32	**8.68**	1.53	**5.46**
Oleic acid	7.51	**28.11**	4.96	**17.56**
Stearic acid	7.35	**27.52**	4.86	**17.07**
Palmitic acid	7.41	**27.75**	4.90	**19.10**
Sum	26.71	**100**	n/a	n/a

Thus, cells cultured in maturation medium receive $5.03*10^{-3}$ mM alpha-linolenic acid, $5.46*10^{-3}$ mM linoleic acid, $1.76*10^{-2}$ mM oleic acid, $1.71*10^{-2}$ mM stearic acid, and $1.91*10^{-2}$ mM palmitic acid.

3.2 Altered contractile function in diseased hiPSC-CMs upon fibrate treatment

To examine the beating pattern of the hiPSC-CM lines, brightfield videos before and after fibrate treatment were quantified. Representative videos of the 1-6 and 1-6-24 lines before treatment can be found in the supplementary information (Supplementary videos 7, 8). The amplitude of the cardiac contractions did not differ significantly before fibrate treatment when comparing the 1-6 (n=10) and 1-6-24 (n=11) cell lines (Figure 2b). Similarly, the beating frequency was insignificant between the diseased (n=11) and isogenic control lines (n=10, Figure 2c). Interestingly, upon fibrate treatment, the amplitude started to change significantly between the cell lines. The amplitude of the bezafibrate-treated 1-6-24 hiPSC-CMs (n=10) is significantly lower compared to the bezafibrate-treated 1-6 cells (n=7, p<0.0001, Figure 3b). No significant difference was observed within one cell line upon fibrate treatment (Figure 3b). The peak time at the 20% threshold before treatment was significantly larger in the 1-6 line (n=11)

compared to its isogenic control (n=11, p<0.001, Figure 2d). After bezafibrate treatment, both the 1-6 (n=6, p<0.01) and 1-6-24 (n=10, p<0.05) lines show a significant reduction in the peak time at the 20% threshold compared to the untreated condition. Moreover, when comparing the fenofibrate condition (n=6) with the untreated condition in the 1-6 line (n=3), the peak time at the 20% threshold is significantly decreased (p<0.05, Figure 3d). Before fibrate treatment, both the systole time (p<0.05, Figure 2e) and the diastole time (p<0.001, Figure 2f) are significantly larger and therefore contribute to a prolonged peak time at the 20% threshold. However, upon fibrate treatment, the systole (Figure 3e) and diastole time at a 20% threshold (Figure 3f) show no significant difference between the 1-6 and 1-6-24 lines. Furthermore, if the peak time before fibrate treatment is assessed at the 50% threshold, a significant increase in the 1-6 (n=11) is seen as compared to the 1-6-24 (n=10, p<0.05, Figure 2g). This also applies to the diastole time of the 1-6 (n=10) and 1-6-24 lines (n=5) at the 50% threshold (p<0.001, Figure 2i). The systole time at the same threshold is not significantly different between the 1-6 (n=11)
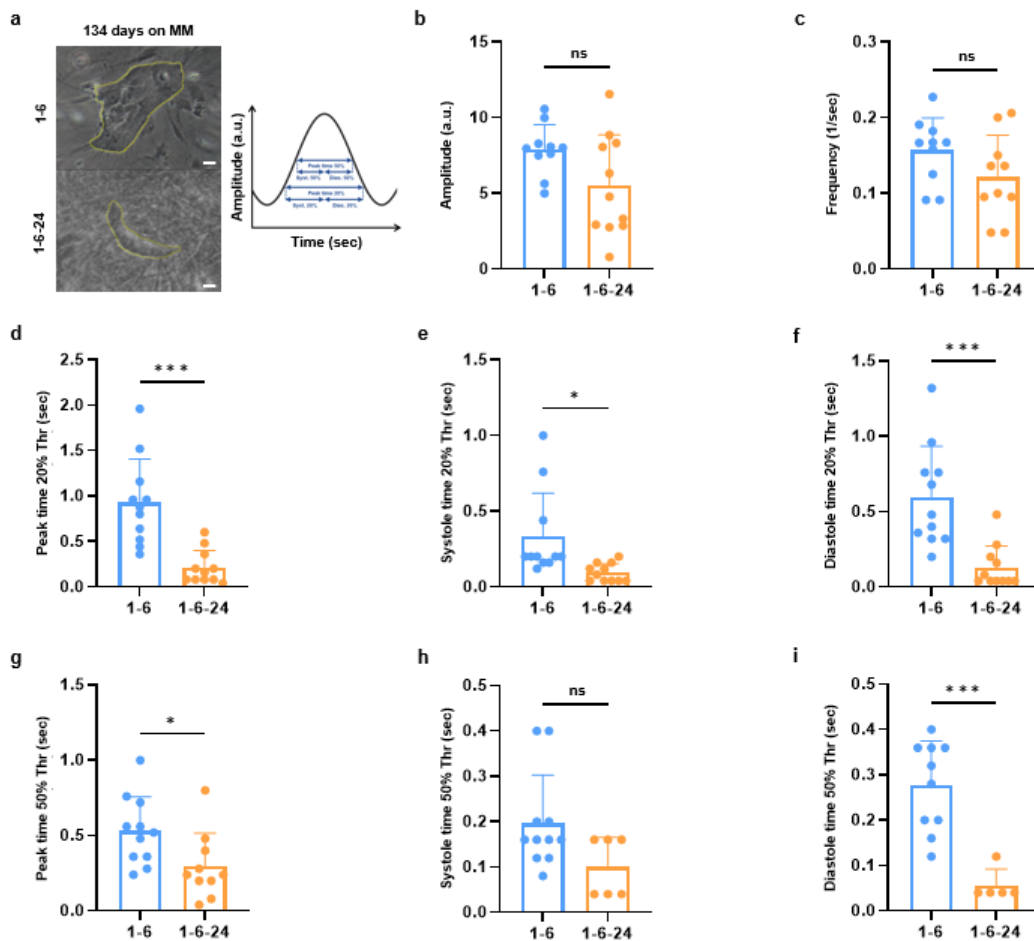
Figure 2: Cardiac contractility in 1-6 and 1-6-24 hiPSC-CMs before fibrate treatment. a: Representative brightfield images of 134-days matured 1-6 and 1-6-24 hiPSC-CMs (10x magnification, scale bar = 50 μm) in combination with a schematic overview displaying a complete cardiac contraction. Peak time, defined as the time it takes to perform a full cardiac contraction (systole + diastole), is presented at two different thresholds: 20% and 50%. Systole time is the time it takes from baseline to reach the peak of the contraction, whereas the diastole time indicates the time it takes for the sarcomeres to relax completely. **b:** Bar graph presenting the amplitude, or the amount of force generated during a cardiac contraction, between the 1-6 (n=10) and 1-6-24 (n=11) cell lines. **c:** Bar graph describing the frequency of cardiac beating between the cell lines (1-6, n=11; 1-6-24, n=10). **d:** Bar graph comparing the peak time at the 20% threshold in 1-6 (n=11) and its isogenic control cells (n=11, p<0.001) **e:** Bar graph presenting the systole time at the 20% threshold in the 1-6 and the 1-6-24 lines (p<0.05). **f:** Bar graph showing the diastole time at the 20% threshold in both lines (1-6, n=11; 1-6-24, n=11, p<0.001). **g:** Bar graph comparing the peak time at the 50% threshold in the 1-6 (n=11) and the 1-6-24 (n=10, p<0.05). **h:** Bar graph depicting the systole time at the 50% threshold in diseased (n=11) and isogenic control (n=6) lines. **i:** Bar graph displaying the time of diastole at the 50% threshold (1-6, n=10; 1-6-24, n=6, p<0.001). Each individual data point describes a single contracting cardiomyocyte. Data are presented as mean +/- SD. Thr = threshold; ns=not significant, *p<0.05, ***p<0.001

and 1-6-24 (n=6) hiPSC-CMs lines (Figure 2h). Upon fibrate treatment, data are not significant between the two cell lines at the 50% threshold (Figure 3g-i). In contrast, the peak time of the bezafibrate-treated 1-6 cardiomyocytes (n=6) at the 50% threshold is significantly shorter compared to the untreated condition (n=2, $p<0.01$, Figure 3g). The systole and diastole time do not show any significant difference at this threshold. Within the 1-6-24 line, a significant difference is observed during the systole of the bezafibrate-treated cells (n=10) compared to the untreated cells (n=5, $p<0.05$, Figure 3h).
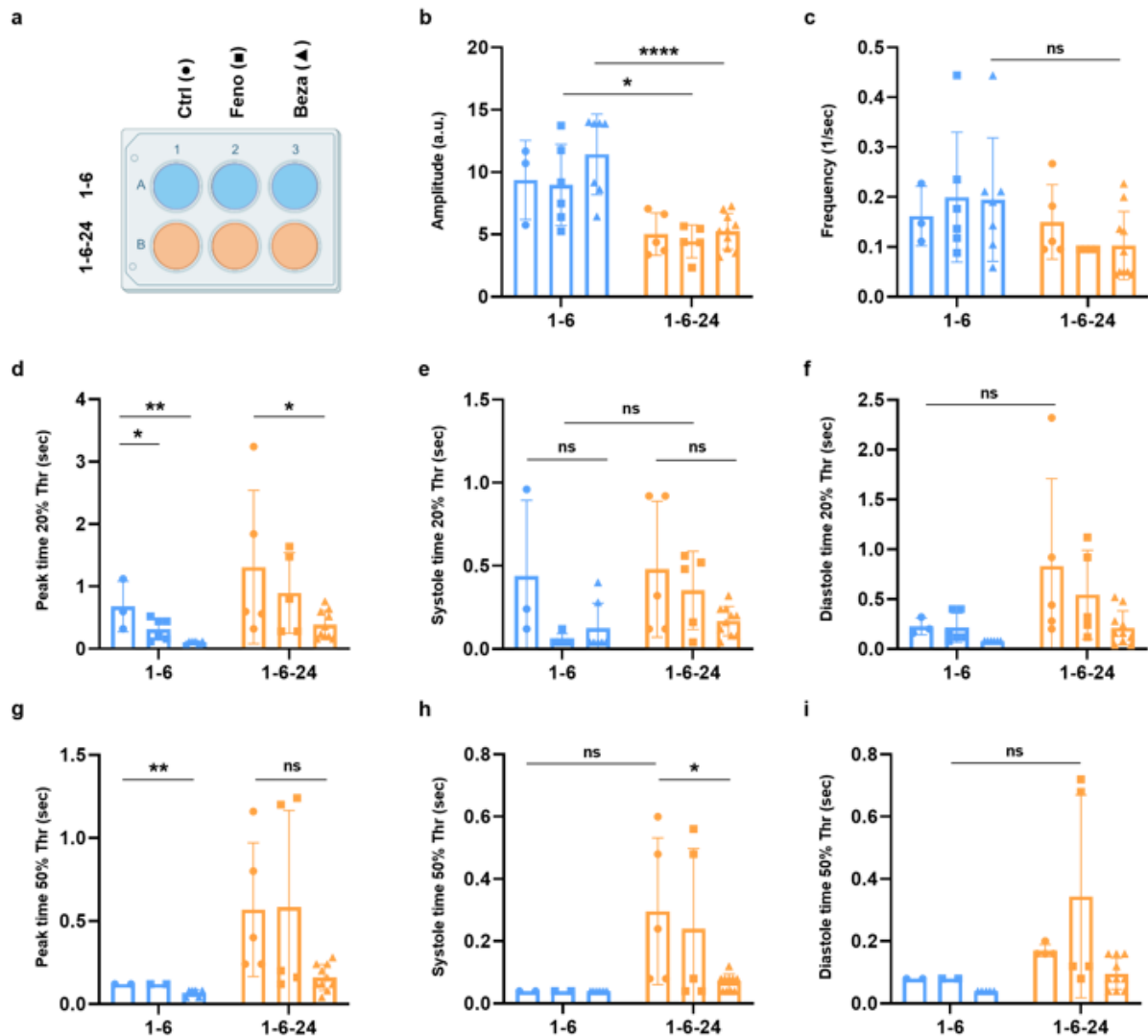
Figure 3: Cardiac contractility in 1-6 and 1-6-24 hiPSC-CMs after fibrate treatment. a: Study design showing the different conditions that are assigned to a specific symbol. **b:** Bar graph presenting the amplitude of the cardiac contraction after fibrate treatment in the 1-6 and 1-6-24 lines. **c:** Bar graph comparing the frequency of cardiac beating between the cell lines upon fibrate treatment. **d:** Bar graph demonstrating the peak time at the 20% threshold. **e:** Bar graph showing the systole time at the 20% threshold. **f:** Bar graph showing the diastole time at the 20% threshold. **g:** Bar graph depicting the peak time at the 50% threshold. **h:** Bar graph displaying the systole time at the 50% threshold. **i:** Bar graph showing the diastole time at the 50% threshold. Each individual data point describes a single contracting cardiomyocyte. Data are presented as mean +/- SD. ● = untreated hiPSC-CMs; ■ = 100 µM fenofibrate incubation for 24h; ▲ = 100 µM bezafibrate incubation for 24h. Thr = threshold; ns = not significant; * $p<0.05$; ** $p<0.01$, *** $p<0.001$, **** $p<0.0001$.

3.3 Aberrant mitochondrial metabolism in diseased hiPSC-CMs compared to isogenic control cells

3.3.1 PPARA levels are boosted by fenofibrate treatment in diseased hiPSC-CMs

To further examine the 1-6 and 1-6-24 hiPSC-CM lines, we evaluated and quantified the protein levels of ACTN2, MYH7, PPARA, and HADHA to investigate the metabolic changes in our HCM model with and without selected metabolic enhancers. To confirm that our cells are cardiomyocytes, we stained for ACTN2. The relative area of ACTN2 does not differ significantly between the 1-6 (n=20) and 1-6-24 (n=11) cell lines before fibrate treatment. Upon fibrate treatment, we observe a significant reduction in the relative area of ACTN2 in the 1-6-24 fenofibrate-treated (n=11) and bezafibrate-treated cells (n=10) compared to the 1-6 hiPSC-CMs treated with fenofibrate (n=19, $p < 0.05$) and bezafibrate (n=19, $p < 0.001$), respectively. Moreover, bezafibrate treatment results in decreased ACTN2 area signals in the 1-6-24 line when compared to the control. The intensity of the ACTN2 signal is significantly enhanced in the untreated (n=21), fenofibrate-treated (n=19), and bezafibrate treated 1-6 cells (n=19) compared to the untreated (n=11, $p < 0.01$), fenofibrate (n=11, $p < 0.0001$), and bezafibrate condition in the 1-6-24 line (n=10, $p < 0.0001$). In the representative IF images, well-developed sarcomeres are observed in the 1-6-24 line, whereas clearly aligned sarcomeres are not visible in the 1-6 line (Figure 4a).

MYH7 area quantification showed no significant differences between the 1-6 and 1-6-24 lines in the untreated (1-6: n=22, 1-6-24: n=15) and fenofibrate-treated conditions (1-6: n=13, 1-6-24: n=14, Figure 4b). However, quantification did reveal a significant increase in the MYH7 area of bezafibrate-treated cells of the 1-6 line (n=22) compared to 1-6-24 cells that received bezafibrate treatment (n=18, $p < 0.05$). The intensity of the MYH7 signal was comparable within the 1-6 line. In the 1-6-24 line, the MYH7 intensity is significantly increased upon bezafibrate treatment (n=18) compared to the control (n=15, $p < 0.05$). Again, sarcomere alignment is scarcely visible in the diseased line (Figure 4b).

Protein level quantification of PPARA did not reveal any significant differences in the PPARA area and intensity between the 1-6 and 1-6-24 cell lines before fibrate treatment. Upon fenofibrate ($p < 0.0001$) and bezafibrate ($p < 0.01$) treatment, however, the relative PPARA area is significantly larger in the 1-6 as compared to the 1-6-24 (Figure 4c). PPARA intensity shows the same significant trend after both fibrate treatments ($p < 0.0001$). Within the 1-6 line, fenofibrate (n=20) boosts the PPARA signal, both the relative area and intensity, significantly compared to the untreated condition (n=20, $p < 0.0001$). In contrast, bezafibrate treatment (n=19) did not result in a significant increase in the relative area and intensity of PPARA in the 1-6 line in comparison to the control (n=20). The PPARA area of the isogenic control cell line showed a significant decrease upon fenofibrate (n=10, $p < 0.05$) and bezafibrate (n=11, $p < 0.01$) treatment compared to the untreated condition (n=11). We observed comparable results for the intensity of the PPARA signal in the fenofibrate (n=10, $p < 0.01$) and bezafibrate-treated (n=11, $p < 0.01$) condition compared to the control (n=11). Representative images of the different conditions in the 1-6 and 1-6-24 cell lines are displayed in Figure 4c.

Quantification of HADHA revealed a significant reduction in the relative area of the 1-6 hiPSC-CMs (n=23) compared to the 1-6-24 line (n=15) before the application of the fibrate treatments ($p < 0.0001$). The HADHA intensity did not show significant differences between the 1-6 (n=23) and 1-6-24 lines (n=15) prior to fibrate incubation. After fenofibrate treatment, the 1-6 cell line shows a significant decrease in the relative HADHA area (n=14, $p < 0.001$), whereas bezafibrate treatment (n=23, $p < 0.01$) causes a significant increase in the relative area of HADHA compared to the untreated 1-6 cells (n=23). Furthermore, the HADHA area of bezafibrate-treated 1-6-24 hiPSC-CMs (n=18) increases significantly when compared to the control (n=15, $p < 0.05$, Figure 4d). After treatment with either fenofibrate (1-6: n=14, 1-6-24: n=14, $p < 0.01$) or bezafibrate (1-6: n=22, 1-6-24: n=18, $p < 0.0001$), the 1-6 HADHA

intensity decreased significantly as compared to the 1-6-24 HADHA intensity. Moreover, we observed that the HADHA intensity of the 1-6 line is reduced upon either fenofibrate (n=13, p<0.001) or bezafibrate (n=22, p<0.001) treatment in comparison to the untreated hiPSC-CMs (n=23). Within the 1-6-24 line, no difference in HADHA intensity was detected between fenofibrate (n=14) or bezafibrate (n=18) treatment compared to the control (n=15).
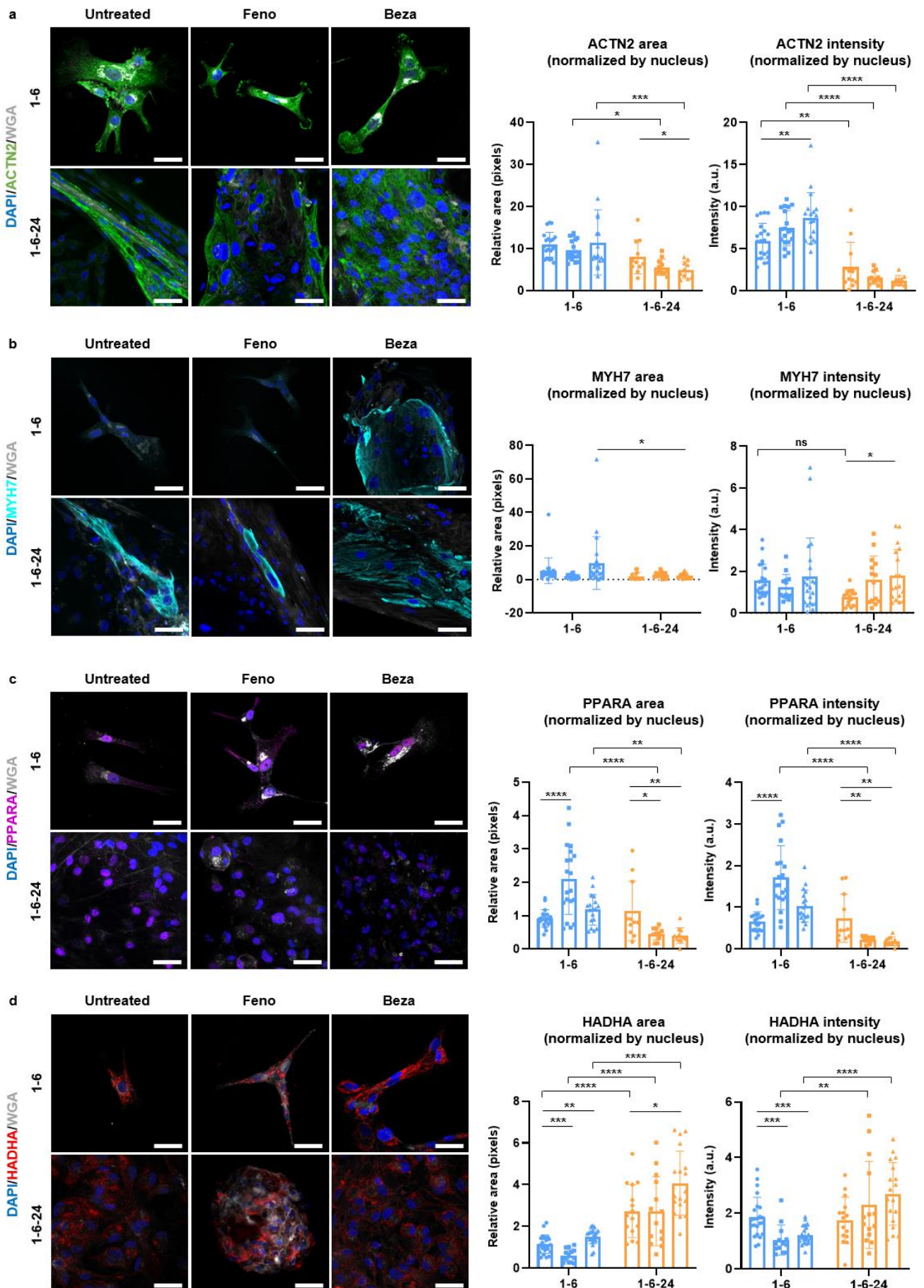
Figure 4: IF staining of (metabolic) candidates in 1-6 and 1-6-24 hiPSC-CMs. Cells were matured for 134 days on Matrigel-coated coverslips and hereafter treated with fibrates for 24 hours. The nuclei were stained by DAPI in blue, whereas membranes were stained with WGA depicted in grey. **a:** Representative IF staining of ACTN2 protein expression in 1-6 and 1-6-24. The area and intensity of the ACTN2 signal, staining sarcomeres in green, were quantified in treated and untreated 1-6 and 1-6-24 hiPSC-CMs. **b:** Representative IF staining of MYH7 in the treated and untreated 1-6 and 1-6-24 cell lines. The area and signal intensity of the IF images of MYH7, staining sarcomere structures in cyan, were quantified. **c:** Representative IF staining displaying PPARA in magenta. Afterward, quantification of the PPARA area and intensity was performed. **d:** Representative IF images of HADHA, staining mitochondrial networks, in red. The bar graphs describe area and signal intensity quantification of HADHA. IF = immunofluorescence, ACTN2 = alpha actinin, MYH7 = myosin heavy chain 7, PPARA = peroxisome proliferator-activated receptor alpha, HADHA = hydroxyacyl-CoA dehydrogenase trifunctional multienzyme complex subunit alpha, WGA = wheat germ agglutinin. Data are presented as +/- SD. Area and signal intensity of the stainings were normalized to the number of nuclei. All IF images were made at 63x magnification. Scale bar = 36.8 μm. • = untreated hiPSC-CMs; ■ = 100 μM fenofibrate incubation for 24h; ▲ = 100 μM bezafibrate incubation for 24h. ns = not significant, *p<0.05, **p<0.01, ***p<0.001, ****p<0.0001.

3.3.2 Upon fenofibrate treatment, KLF15 levels increase significantly in 1-6 and 1-6-24 hiPSC-CMs

As we lacked untreated hiPSC-CMs that were stained for CD36 and KLF15, we could still establish the efficacy of the fibrate treatments relative to each other and between the 1-6 and 1-6-24 cell lines. The CD36 area, normalized to the number of nuclei, was significantly higher in the fenofibrate-treated 1-6-24 cells (n=15) as compared to the fenofibrate-treated 1-6 cells (n=19, p<0.001). The fenofibrate-treated isogenic control cells (n=15) show a significant increase in CD36 area when compared to the bezafibrate-treated 1-6-24 cells (n=14, p<0.001, Figure 5a). Quantification of the CD36 intensity revealed significantly reduced signals in the fenofibrate (n=15) and bezafibrate-treated 1-6-24 cells (n=15) compared to the signals in fenofibrate-treated (n=20, p<0.0001) and bezafibrate-treated 1-6 cells (n=19, p<0.05), respectively.

KLF15 area analysis showed that bezafibrate treatment in the isogenic control line (n=15) results in a significantly reduced signal when compared to bezafibrate-treated diseased cells (n=20, p<0.01). Within the 1-6 cell line, bezafibrate treatment causes a significantly lower KLF15 area signal when compared to the fenofibrate-treated hiPSC-CMs (n=20, p<0.05). The area of bezafibrate-treated 1-6-24 cells is significantly decreased compared to the area of the fenofibrate-treated 1-6-24 cells as well (n=15, p<0.0001). Examination of the fibrate treatments on KLF15 intensity showed that both fenofibrate-treated (n=15) and bezafibrate-treated 1-6-24 hiPSC-CMs (n=15) have a decreased intensity in comparison to the fenofibrate-treated (n=20, p<0.01) and bezafibrate-treated cells in the 1-6 line (n=20, p=0.05), respectively. Fibrate treatment in both the 1-6 (p<0.001) and 1-6-24 lines (p<0.0001) revealed a significant increase upon fenofibrate treatment compared to bezafibrate-treated cells.
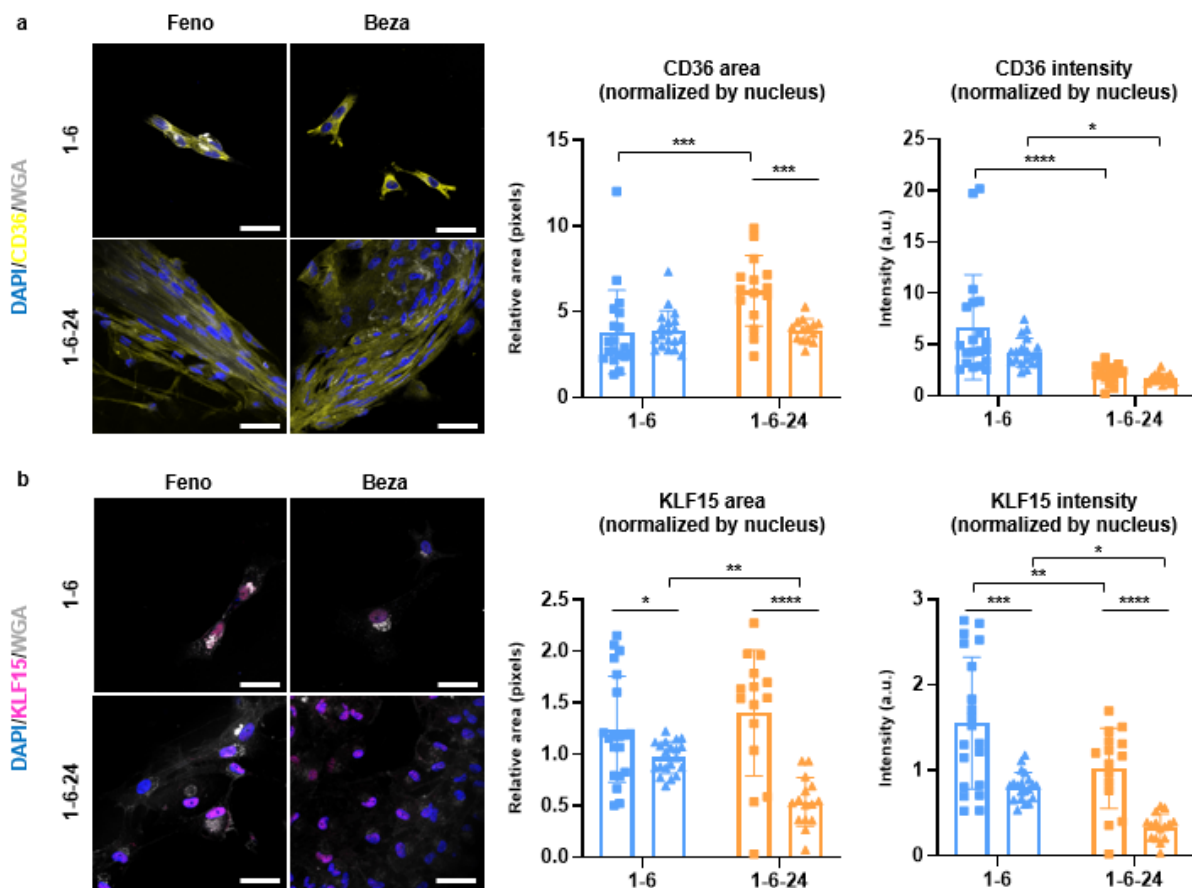
Figure 5: IF staining of metabolic candidates in fibrate-treated 1-6 and 1-6-24 hiPSC-CMs. Cells were matured for 134 days on Matrigel-coated coverslips and hereafter treated with fibrates for 24 hours. The nuclei were stained by DAPI in blue, whereas membranes were stained with WGA depicted in grey. **a:** Representative IF staining CD36 in 1-6 and 1-6-24 hiPSC-CMs after either fenofibrate or bezafibrate treatment. Bar graphs show the area and intensity of the yellow CD36 signal in the IF images that was quantified. **b:** Representative IF staining of KLF15 in fenofibrate and bezafibrate treated 1-6 and 1-6-24 hiPSC-CMs. Bar graphs present the area and signal intensity that was quantified. IF = immunofluorescence, CD36 = Cluster of Differentiation 36, KLF15 = Krüppel-like factor 15. Data are presented as +/- SD. Area and signal intensity of the stainings were normalized to the number of nuclei. All IF images were made at 63x magnification. Scale bar = 36.8 μm. ■ = 100 μM fenofibrate incubation for 24h; ▲ = 100 μM bezafibrate incubation for 24h. ns = not significant, *p<0.05, **p<0.01, ***p<0.001, ****p<0.0001

3.4 Mitochondrial stress test revealed decreased FAO in diseased hiPSC-CMs

To assess metabolic activity, live 1-16, CVI273, and 1-16-40.5 cells underwent the mitochondrial stress test in which sequential injections with metabolic inhibitors were performed and several parameters could be assessed (Figure 6a).[47] Representative images of the cell lines were made prior to the analysis and showed variable densities (Figure 6b). Before the addition of any stressors, basal respiration and basal glycolysis was determined by measuring the OCRs and ECARs, respectively (Figure 6c, 6e). We observed a significantly decreased basal respiration in the diseased cell line (n=27) as compared to the CVI273 (n=27, p<0.0001) and isogenic control cells (n=6, p<0.05, Figure 6d). Furthermore, the basal OCR of the CVI273 cells (n=27) was significantly higher when compared to the basal OCR of the isogenic control cells (n=6, p<0.01). Upon injection of oligomycin, a major decrease in aerobic ATP production is observed in the CVI273 and isogenic control cells while the 1-16 line shows a slight decrease (Figure 6c). As a result, no significant differences in mitochondrial ATP production are detected between the 1-16 (n=26), CVI273 (n=27), and 1-16-40.5 cell lines (n=6, Figure 6d). FCCP injection induces a minor response

in 1-16 hiPSC-CMs, but a major response in the control lines (Figure 6c). This translates into a significantly enhanced maximal respiration in the CVI273 (n=27) and 1-16-40.5 cells (n=6) compared to the 1-16 cell line (n=26, p<0.0001, Figure 6d). ECAR analysis revealed significantly reduced basal glycolysis in the 1-16 line (n=27) compared to the CVI273 (n=26, p<0.0001) and 1-16-40.5 lines at baseline (n=6, p<0.05, Figure 6f). Inhibition with oligomycin increased the glycolytic capacity of the cell lines. Again, the diseased line (n=27) has a significantly lower ECAR compared to the CVI273 (n=27, p<0.0001) and 1-16-40.5 (n=6, p<0.01) controls upon oligomycin addition. In addition, the CVI273 cells respond significantly stronger to the oligomycin injection compared to the 1-16-40.5 cells (n=6, p<0.01, Figure 6f). The same pattern for FCCP sensitivity is observed after FCCP injection. As no normalization methods were applied, absolute values before and after treatment with the metabolic inhibitions were taken for the analyses.
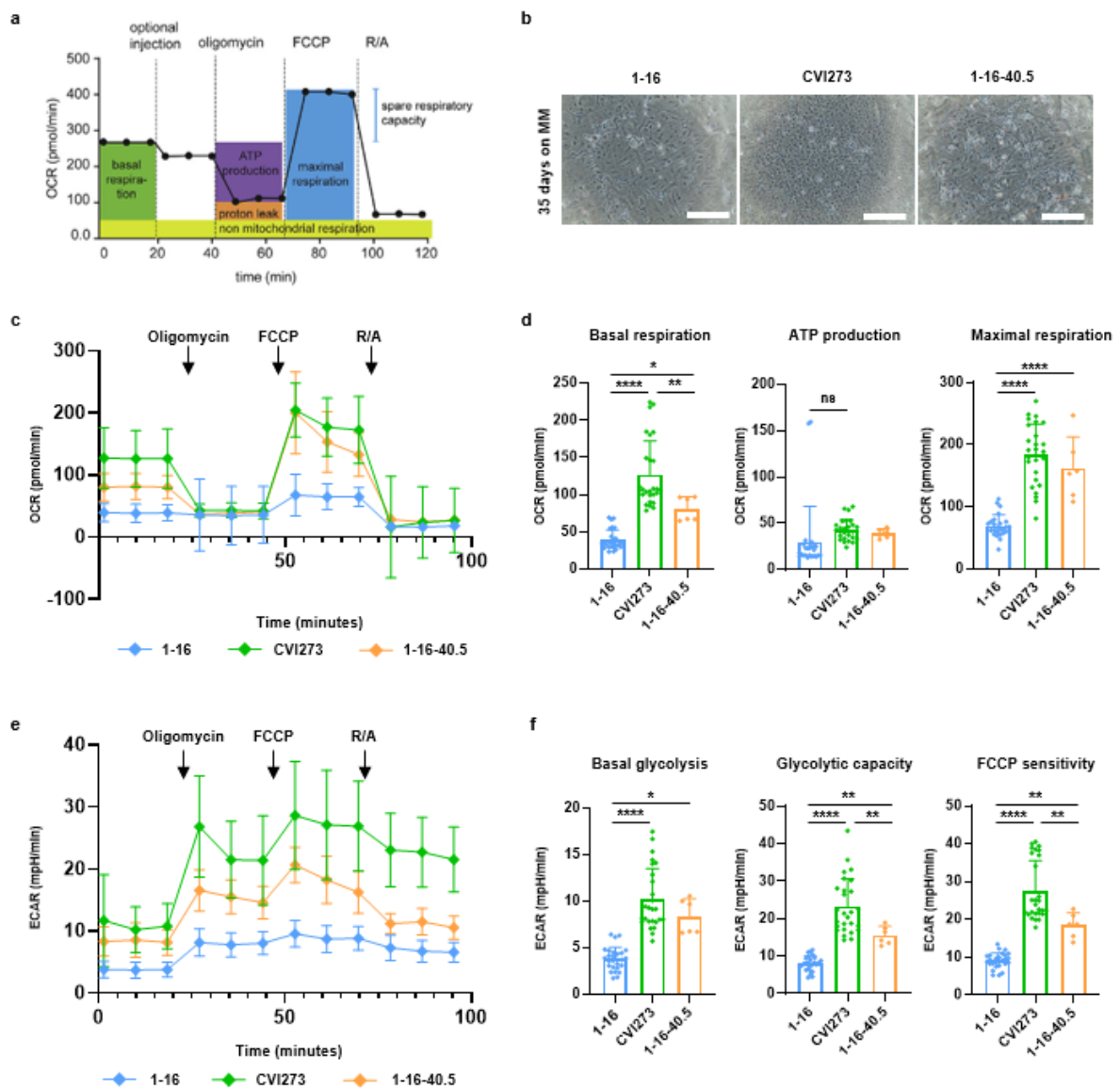
Figure 6: Mitochondrial stress test on 1-16, CVI273, and 1-16-40.5 cells. a: Mitochondrial stress test profile depicting the parameters that can be assessed. Adapted from Ludikhuize et al.[47] **b:** Representative brightfield images of the 1-16, CVI273, and 1-16-40.5 cell lines made at 4x magnification while focusing on the center of the microplate well. Scale bar = $1.32*10^5$ μm. **c:** OCR in the 1-16, CVI273, and 1-16-40.5 lines upon injection of different metabolic inhibitors. **d:** Bar graphs showing the basal respiration, ATP production, and maximal respiration of the 1-16, CVI273, and 1-16-40.5 cell lines. **e:** ECAR in the 1-16, CVI273, and 1-16-40.5 lines upon injection of different metabolic inhibitors. **f:** Bar graphs displaying the basal glycolysis, glycolytic capacity, and FCCP sensitivity in the 1-16, CVI273, and 1-16-40.5 cell lines. OCR = oxygen consumption rate, ECAR = extra cellular acidification rate, FCCP = carbonyl cyanide-4 (trifluoromethoxy) phenylhydrazone, R/A = rotenone/antimycin A. Data are presented as +/- SD. *p<0.05, **p<0.01, ****p<0.0001.

3.5 Significantly different areas in the 1-6 and 1-6-24 3D cardiac clusters

3D cardiac clusters observed in both cell lines were quantified using the ImageJ output (area, width, length) and the Z-stack data (Z-size). As visible in the representative brightfield images (Figure 7a), cardiac cluster areas are significantly bigger in the 1-6-24 line (n=59, p<0.001) when compared to the 1-6 line (n=64, Figure 7b). To investigate the growth of these clusters over time, we further divided the culturing periods into four phases, namely the early (0-30 days), mid (30-60 days), late (60-90 days), and latest (90-135 days) phase of maturation. We observed that the areas of the 1-6-24 clusters (n=20) are significantly increased in the latest stage of maturation compared to the early stage (n=11, p<0.05). In both lines, no significant differences were found between the early and mid, or mid and late stages of maturation. Areas of the cardiac clusters in the same phase of maturation did not differ significantly between the 1-6 and 1-6-24 line (Figure 7c). Additionally, a gradual increase in the areas of the 1-6-24 clusters and a slight decrease in the 1-6 clusters can be seen. Besides, the slopes of the corresponding 1-6 and 1-6-24 equations are significantly different (p<0.01, Figure 7d). Next, the structure of the cardiac clusters, defined by the ratio of the width and length of the cluster, was examined. Analysis of the structure of cardiac clusters, both independent of maturation time (Figure 7e) and during different stages of maturation (Figure 7f), did not result in a significant difference.

Besides observing the cardiac clusters throughout the maturation of the hiPSC-CMs, we quantified clusters that were still present after fixation and IF staining of the 1-6 and 1-6-24 line. Interestingly, upon fibrate-treatment, an increased number of cardiac clusters in the coverslip, based on sarcomere-positive *MYH7* staining, was identified when compared to the untreated condition. We also observed increased sarcomere-positive clusters in the 1-6-24 cells compared to the 1-6 hiPSC-CMs (Figure 7g). Moreover, a Z-size comparison of the different conditions (untreated, fenofibrate-treated, bezafibrate-treated) revealed that the fenofibrate-treated 1-6 (n=4) clusters are significantly thicker than the 1-6-24 clusters (n=12) that are treated with fenofibrate as well. Within the 1-6-24 line, treatment with bezafibrate (n=36) resulted in significantly thicker clusters, based on MYH7 sarcomere staining, compared to the untreated condition (n=1, p<0.05, Figure 7h).
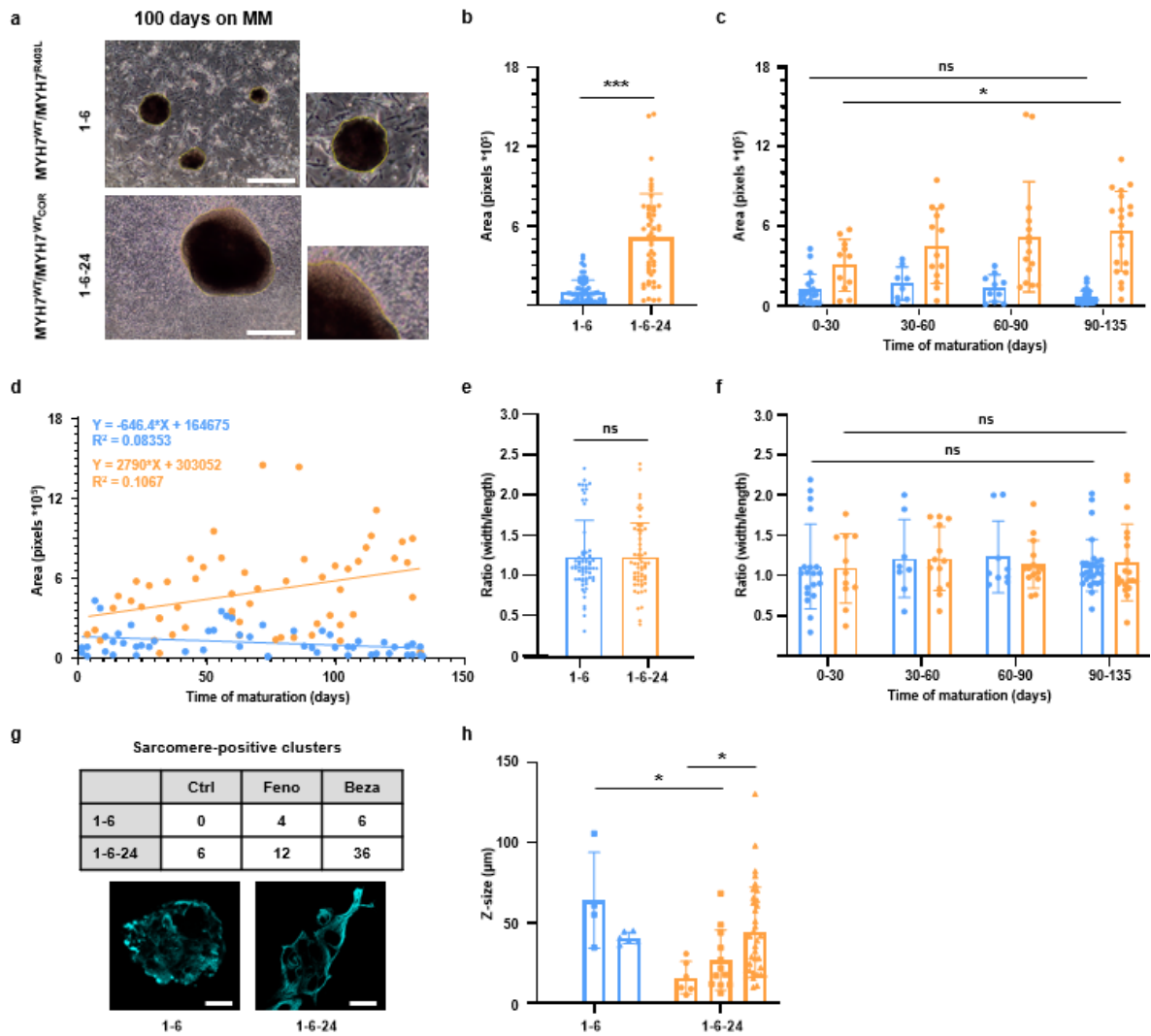
Figure 7: Cardiac cluster quantification. a: Representative brightfield images showing 3D cardiac clusters in culture, 100 days on maturation medium (MM). The yellow line indicates the areas manually selected with ImageJ. Scale bar = 500 pixels ($1.32*10^5$ µm). **b**: Bar graph comparing the areas of the clusters observed in the 1-6 line (n=64) with the 1-6-24 line (n=59). *** p <0.001. **c**: Bar graph presenting the area changes of the 1-6 and 1-6-24 clusters during different stages (early, mid, late, latest) of maturation. **d**: Correlation plot describing the area changes throughout the 135 days of maturation. **e**: Bar plot comparing the structure, the ratio of the width and length, of the cardiac clusters in both lines (1-6, n=65; 1-6-24, n=59). **f**: Bar graph presenting the structural changes of the 1-6 and 1-6-24 cardiac clusters throughout the different maturation stages. **g**: Table showing the effect of fibrate treatment on the number of sarcomere-positive clusters after immunofluorescent staining. Representative images of the MYH7 stained fenofibrate-treated hiPSC-CMs are included. Scale bar = 36.8 µm. **h**: Bar graph comparing the thickness of the 3D cardiac clusters upon fibrate treatment after immunofluorescent staining. Data is compared with the untreated condition. Each individual data point describes a cardiac cluster. ● = untreated hiPSC-CMs; ■ = 100 µM fenofibrate incubation for 24h ▲ = 100 µM bezafibrate incubation for 24h. Data are presented as mean +/- SD. MM = maturation medium, ns = not significant, * p<0.05, **p<0.01, *** p<0.001

4. Discussion

In this study, we present for the first time a comprehensive overview demonstrating all components throughout the long-term cultivation period of hiPSC-CMs with the R403L variant in the *MYH7* gene and its isogenic control line. Hereafter, we validated our model by conducting functional assays that showed disturbed contractile function and decreased FAO in the diseased line when compared to the isogenic control line. Next, we treated the cells with metabolic modulators, either enhancers (fibrates) or inhibitors (oligomycin, FCCP, R/A) and examined the cellular response at the functional level and protein expression level. Overall, the experiments demonstrated that the diseased cells responded better to fenofibrate treatment than bezafibrate treatment and they showed a minor response upon addition of the inhibitory compounds when compared to both the isogenic and wildtype control cell lines.

Functional characterization of our *in vitro* model showed a slight trend towards an increase in the amplitude of the cardiac contraction in the 1-6 line compared to the 1-6-24 line, indicating that the contractile power is comparable between the cell lines. Besides contractile dysfunction, hypertrophy of the cells is another key hallmark of HCM.[48] A recent study performed by Roest *et al.* detected a significant increase in force generation and cardiomyocyte hypertrophy in hiPSC-CMs carrying the p.P710R variant in the *MYH7* gene compared to their CRISPR/Cas9 corrected isogenic control line after correcting for cell size.[48] We also observed a larger cell size in the diseased cells compared to the isogenic control cells. However, quantification was not performed due to time limitations. Therefore, in future studies, performing flow cytometry to correct for cardiomyocyte size would be recommended.[49] We did not observe any significant differences in the beating frequency between the diseased and isogenic hiPSC-CMs lines, suggesting no hypo- or hypercontractility in the 1-6 line. However, only one or two contractions were generally captured during the recorded time frame of 15-20 seconds. Therefore, in order to accurately measure any possible abnormalities in the beating frequency of single cardiomyocytes, a longer recording time frame of around 60 seconds, allowing the opportunity to capture more complete cardiac contractions, should be considered. Literature reports conflicting evidence regarding systolic (dys)function in HCM. While the hiPSC-CMs with the p.P710R and p.R403Q variants display hypercontractility, systolic function is often preserved in HCM.[48,50,51] Notably, we reported a significant increase in the duration of the cardiac contractions at the 20% threshold in diseased hiPSC-CMs compared to the cells in the 1-6-24 line. This finding aligns with studies that examined cardiac contractility in 3D cardiac microtissues and HCM patients.[51,52] In contrast to these studies that only reported prolonged relaxation, we also observed a significant increase in the systole time of 1-6 hiPSC-CMs in the peak time at the 20% threshold.[51] Upon fibrate treatment, this increase is restored again. However, due to a small sample size and large standard deviation, it is unclear if the decreased contraction time is due to a decreased systole or diastole time. Future studies should point out whether including a larger sample size and a larger recording time frame results in a significantly altered systole or diastole time in HCM patients carrying the *MYH7* mutation. The peak time at the 50% threshold showed a similar pattern as the results of the cardiac contractility at the 20% threshold.

Besides contractile function, a significantly decreased mitochondrial respiration in diseased cells as compared to the wildtype and isogenic control cells by measuring their basal OCRs and ECARs using the seahorse assay was shown. Depending on the amount of cells present in the microplate well, a basal OCR for highly oxidative cells, such as cardiomyocytes, varies between 100-200 pmol O_2/min, which aligns with the OCR of our CVI273 control cells.[49,53] Similarly, upon injection of the metabolic inhibitors to the 1-16, CVI273, and 1-16-40.5 cells, major differences were observed between the diseased and control cells. The maximal respiration of the 1-16 cells was significantly decreased in comparison to the control lines, indicating limited oxidative capacity in the diseased cells. Interestingly, the findings in the 1-16 cells contradict with several papers indicating elevated basal and maximal OCRs in HCM models

and hiPSC-CMs lines with an *MYH7* variant as compared to control lines.[49,54,55] This raises questions whether the diseased cell line is metabolically inactive or contains a lower number of live cells. Although we seeded the same number of cells at the start of the maturation, already major differences in cell density were observed between the cell lines after 30 days of maturation. Therefore, the obtained OCRs should be further normalized by cell numbers, either by counting the number of cells prior to the start of the seahorse assay using the Countess II FL Automated Cell counter or IF staining of cell membrane markers. The ECAR, on the other hand, reflects the changes in the OCR upon oligomycin and FCCP injection. After suppression of the ATP synthase or uncoupling of the mitochondrial oxidative phosphorylation, elevated glycolytic capacity is observed in both diseased and control cell lines as visible by the increase in the ECARs. Again, the 1-16 line is less responsive to the inhibitory agents as compared to the CVI273 and 1-16-40.5 cell lines.[49,54,55]

Upon metabolic enhancement with fibrates, a significant increase in the contractile force generated by the 1-6 line compared to the 1-6-24 line was observed, implying that the fibrates cause an increase in the energy availability that the cells can use to overcome the energy deficit seen in HCM pathophysiology. The beating frequency within the 1-6 and 1-6-24 cell lines did not change upon fibrate treatment while the peak time at the 20% threshold was reduced in the 1-6 and 1-6-24 line after bezafibrate treatment. Diseased cells also responded to fenofibrate treatment, thereby restoring the increased peak time at the 20% threshold that was observed before the application of the treatment. Large standard deviations and small sample sizes were followed by unreliably and mostly insignificant results in the diastole and systole times at both the 20% and the 50% threshold. However, further research on the effect of fibrate treatment on cardiac contractile function is required. Fenofibrate-treated 1-6 hiPSC-CMs also showed a significantly increased PPARA protein level. This is in line with previous reports showing increased PPARA expression in fenofibrate-treated neonatal rat cardiomyocytes (10 µM for 4 hours) and left ventricles of male rats (100 mg/kg/day for 8 weeks), as established by western blotting.[56,57] Interestingly, Jen HL *et al.* even demonstrated that addition of fenofibrate (100 µM) diminished cardiac hypertrophy in a human cardiomyocyte model in a PPARA mediated fashion.[23] *In vitro* work by Zhu Tang *et al.* showed significant upregulation of PPARA levels after bezafibrate treatment (100 mg/kg/day for 7 weeks), thereby attenuating cardiac hypertrophy in neonatal rat ventricular cardiomyocytes.[24] However, our data showed that bezafibrate treatment did not have any impact on restoring PPARA levels in the diseased cells. Although we applied similar fibrate concentrations, crystal-like structures were observed upon fibrate treatment (Supplementary image 5). Taken all together, these results suggest that optimizations of the fibrate concentrations and incubate times in hiPSC-CMs carrying the *MYH7_R403L* variant are still necessary. IF staining of mitochondrial networks revealed significant downregulation of HADHA on a protein level upon fibrate treatment in diseased cells with the *MYH7* variant compared to isogenic control cells. This is confirmed by findings and inhouse data of HCM hearts carrying the *PLNR14del* or *MYBPC3* variant of which the latter was previously reported by Pei *et al.*.[4] Within the 1-6 cell line, HADHA levels are significantly increased upon bezafibrate treatment, but this does not result in complete restoration of a healthy phenotype. Inconsistently, fenofibrate treatment significantly enhanced CD36 and KLF15 levels in diseased and isogenic control hiPSC-CMs as compared to bezafibrate treatment.[58] Diseased cells stained for ACTN2 and MYH7 show poor sarcomere alignment, suggesting sarcomere disarray in our HCM model. Remarkably, the isogenic control line shows significantly lower ACTN2 levels. To further validate the results, it would be recommended to add an additional normalization method or confirm the findings by using western blotting or proteomics.

One of the main limitations of this study is our 1-6-24 isogenic control line. We optimized the MYH7 staining protocol using the 1-16-40.5 isogenic control line and observed acceptable MYH7 signals.

However, approximately 50% of the 1-6-24 cells did not contain clear MYH7 signals. As this arose confusion, we decided to perform Sanger sequencing on the 1-6-24 and 1-16-40.5 isogenic control lines, which revealed that the causative *MYH7* variant had returned in the 1-6-24 line while the initial variant in the 1-16-40.5 line was well-corrected (Supplementary file 14). Currently, we are investigating how the recurrence of the *MYH7* variant was possible, but that is beyond the scope of this project.

Another major limitation is the maturation status of the cell lines. Maturing hiPSC-CMs is challenging and can be achieved by applying a culturing medium supplemented with a high fatty acid concentration as described before.[28,29,59] While most researchers have been culturing the hiPSC-CMs in a maturation medium for 30 to 40 days, we matured the 1-6 and 1-6-24 lines up till 135 days to mimic a more advanced stage of the disease.[28,29,59] Additionally, we cultured the cells using a novel maturation medium that enhanced long-term stability and sarcomere organization.[28] Media component characterization revealed that the approximate concentrations of FFAs in the maturation medium are comparable with the physiological plasma fatty acid levels in humans, validating that the fatty acid supply is not causing additional FAO stimulation.[60] Yet, strategies to enhance the maturity of hiPSC-CMs could be further improved. For instance, a promising approach for hiPSC-CMs maturation is cultivation on combinatorial polymer matrices that mimic the extracellular matrix and improve mitochondrial function and contractility.[61] Upon long-term maturation we also observed spontaneously beating 3D cardiac clusters in both the 1-6 and 1-6-24 lines. While the cardiac clusters of the diseased line deteriorated at the end of the maturation period, the 1-6-24 clusters remained stable. Additional studies should be performed to check whether the cardiac clusters represent a physiologically relevant 3D *in vitro* model. Interestingly, the size of the cardiac clusters is comparable with the size of engineered heart tissues which are considered an advanced *in vitro* model.[62] Intriguingly, Murphy *et al.* showed that hiPSC-CM maturation is promoted by treatment with the PPARA agonist WY14643, thereby putting the fibrate treatment that we applied in a different perspective.[63]

In conclusion, we show aberrant contractile function, impaired myocardial energy metabolism, and sarcomere disarray in a hiPSC-CM model carrying the *MYH7_R403L* variant. The diseased lines respond to the metabolic enhancer fenofibrate, while a minor response was provoked upon metabolic inhibition. The fibrate administration protocol, including the time and concentration, in *in vitro* studies, should be further optimized before *in vivo* implementation. Additionally, routine sequencing of hiPSC-CM lines, for instance using next generation sequencing, and finding an ideal hiPSC-CM maturation strategy are key to progress in cardiovascular research.

5. Acknowledgements

6. References

1. Crilley, J. G. *et al.* Hypertrophic cardiomyopathy due to sarcomeric gene mutations is characterized by impaired energy metabolism irrespective of the degree of hypertrophy. *J. Am. Coll. Cardiol.* **41**, 1776–1782 (2003).

2. Toepfer, C. N. *et al.* Myosin Sequestration Regulates Sarcomere Function, Cardiomyocyte Energetics, and Metabolism, Informing the Pathogenesis of Hypertrophic Cardiomyopathy. *Circulation* 828–842 (2020) doi:10.1161/CIRCULATIONAHA.119.042339.

3. Viola, H. M. & Hool, L. C. Impaired calcium handling and mitochondrial metabolic dysfunction as early markers of hypertrophic cardiomyopathy. *Arch. Biochem. Biophys.* **665**, 166–174 (2019).

4. Pei, J. *et al.* Multi-omics integration identifies key upstream regulators of pathomechanisms in hypertrophic cardiomyopathy due to truncating MYBPC3 mutations. *Clin. Epigenetics* **13**, (2021).

5. Witjas-Paalberends, E. R. *et al.* Mutations in MYH7 reduce the force generating capacity of sarcomeres in human familial hypertrophic cardiomyopathy. *Cardiovasc. Res.* **99**, 432–441 (2013).

6. Marian, A. J. & Braunwald, E. Hypertrophic cardiomyopathy: Genetics, pathogenesis, clinical manifestations, diagnosis, and therapy. *Circ. Res.* **121**, 749–770 (2017).

7. Saltzman, A. J. *et al.* Short communication: The cardiac myosin binding protein C Arg502Trp mutation: A common cause of hypertrophic cardiomyopathy. *Circ. Res.* **106**, 1549–1552 (2010).

8. Velicki, L. *et al.* Genetic determinants of clinical phenotype in hypertrophic cardiomyopathy. *BMC Cardiovasc. Disord.* **20**, (2020).

9. Hamosh, A. & McKusick, V. A. 160760: Myosin, Heavy Chain 7, Cardiac Muscle, Beta; Myh7. *Online Mendelian Inheritance in Man* https://www.omim.org/entry/160760 (1986).

10. Richard, P. *et al.* Hypertrophic cardiomyopathy: Distribution of disease genes, spectrum of mutations, and implications for a molecular diagnosis strategy. *Circulation* **107**, 2227–2232 (2003).

11. Chung, M.-W., Tsoutsman, T. & Semsarian, C. *Hypertrophic cardiomyopathy: from gene defect to clinical disease. Cell Research* vol. 13 http://www.cell-research.com (2003).

12. Tuohy, C. V., Kaul, S., Song, H. K., Nazer, B. & Heitner, S. B. Hypertrophic cardiomyopathy: the future of treatment. *Eur. J. Heart Fail.* **22**, 228–240 (2020).

13. Lekaditi, D. & Sakellaropoulos, S. Myosin Modulators: The New Era of Medical Therapy for Systolic Heart Failure and Hypertrophic Cardiomyopathy. *Cardiol. Res.* **12**, 146–148 (2021).

14. Batzner, A., Schäfers, H.-J., Borisov, K. V. & Seggewiß, H. Hypertrophic Obstructive Cardiomyopathy. *Dtsch. Arztebl. Int.* (2019) doi:10.3238/arztebl.2019.0047.

15. Jung, W. I. *et al.* 31P NMR spectroscopy detects metabolic abnormalities in asymptomatic

patients with hypertrophic cardiomyopathy. *Circulation* **97**, 2536–2542 (1998).

16. Ranjbarvaziri, S. *et al.* Altered Cardiac Energetics and Mitochondrial Dysfunction in Hypertrophic Cardiomyopathy. *Circulation* **144**, 1714–1731 (2021).

17. Li, X. *et al.* Weighted gene co-expression network analysis revealed key biomarkers associated with the diagnosis of hypertrophic cardiomyopathy. *Hereditas* **157**, (2020).

18. Schuldt, M. *et al.* Proteomic and Functional Studies Reveal Detyrosinated Tubulin as Treatment Target in Sarcomere Mutation-Induced Hypertrophic Cardiomyopathy. *Circ. Hear. Fail.* **14**, E007022 (2021).

19. Coats, C. J. *et al.* Proteomic Analysis of the Myocardium in Hypertrophic Obstructive Cardiomyopathy. *Circ. Genomic Precis. Med.* **11**, (2018).

20. Prosdocimo, D. A. *et al.* KLF15 and PPAR α Cooperate to regulate cardiomyocyte lipid gene expression and oxidation. *PPAR Res.* **2015**, (2015).

21. d'Emden, M. C. *et al.* Favourable effects of fenofibrate on lipids and cardiovascular disease in women with type 2 diabetes: results from the Fenofibrate Intervention and Event Lowering in Diabetes (FIELD) study. *Diabetologia* **57**, 2296–2303 (2014).

22. Poole, R. *Improving cardiovascular outcomes in type 2 diabetes*. *Practitioner* vol. 166 http://diabetesjournals.org/care/article-pdf/21/4/641/664270/21-4-641.pdf (2022).

23. Jen, H.-L., Yin, W.-H., Chen, J.-W. & Lin, S.-J. Endothelin-1-Induced Cell Hypertrophy in Cardiomyocytes is Improved by Fenofibrate: Possible Roles of Adiponectin. *J Atheroscler Thromb* **24**, 508–517 (2017).

24. Xu, S. C., Ma, Z. G., Wei, W. Y., Yuan, Y. P. & Tang, Q. Z. Bezafibrate Attenuates Pressure Overload-Induced Cardiac Hypertrophy and Fibrosis. *PPAR Res.* **2017**, (2017).

25. Buikema, J. W., Van Der Meer, P., Sluijter, J. P. G. & Domian, I. J. Engineering myocardial tissue: The convergence of stem cells biology and tissue engineering technology. *Stem Cells* **31**, 2587–2598 (2013).

26. Li, J., Feng, X. & Wei, X. Modeling hypertrophic cardiomyopathy with human cardiomyocytes derived from induced pluripotent stem cells. *Stem Cell Res. Ther.* **13**, (2022).

27. Vučković, S. *et al.* Characterization of cardiac metabolism in iPSC-derived cardiomyocytes: lessons from maturation and disease modeling. *Stem Cell Res. Ther.* **13**, (2022).

28. Feyen, D. A. M. *et al.* Metabolic Maturation Media Improve Physiological Function of Human iPSC-Derived Cardiomyocytes. *Cell Rep.* **32**, 107925 (2020).

29. Horikoshi, Y. *et al.* Fatty acid-treated induced pluripotent stem cell-derived human cardiomyocytes exhibit adult cardiomyocyte-like energy metabolism phenotypes. *Cells* **8**, (2019).

30. Ronaldson-Bouchard, K. *et al.* Advanced maturation of human cardiac tissue grown from pluripotent stem cells. *Nature* **556**, 239–243 (2018).

31. Carson, D. *et al.* Nanotopography-Induced Structural Anisotropy and Sarcomere Development in Human Cardiomyocytes Derived from Induced Pluripotent Stem Cells. *ACS Applied Materials and Interfaces* vol. 8 21923–21932 (2016).

32. Okita, K. *et al.* A more efficient method to generate integration-free human iPS cells. *Nat. Methods* **8**, 409–412 (2011).

33. Lian, X. *et al.* Directed cardiomyocyte differentiation from human pluripotent stem cells by modulating Wnt/β-catenin signaling under fully defined conditions. *Nat. Protoc.* **8**, 162–175 (2013).

34. Fontaine, V. *et al.* Generation of iPSC line from MYH7 R403L mutation carrier with severe hypertrophic cardiomyopathy and isogenic CRISPR/Cas9 corrected control. *Stem Cell Res.* **52**, (2021).

35. Fan, Y. *et al.* Wnt/β-catenin-mediated signaling re-activates proliferation of matured cardiomyocytes. *Stem Cell Res. Ther.* **9**, (2018).

36. Grune, T., Ott, C., Häseli, S., Höhn, A. & Jung, T. the 'MYocYteR'-convert cellular and cardiac contractions into numbers with imageJ. doi:10.1038/s41598-019-51676-x.

37. Technical Resources - 21875 RPMI 1640. https://www.thermofisher.com/nl/en/home/technical-resources/media-formulation.187.html.

38. Technical Resources 11966 - DMEM, no glucose. https://www.thermofisher.com/nl/en/home/technical-resources/media-formulation.49.html.

39. Technical Resources 11140 - MEM Non-Essential Amino Acids solution. https://www.thermofisher.com/nl/en/home/technical-resources/media-formulation.165.html.

40. Maas, R. G. C. *et al.* Massive expansion and cryopreservation of functional human induced pluripotent stem cell-derived cardiomyocytes. *STAR Protoc.* **2**, 100334 (2021).

41. Technical Resources - B27 Serum-free Supplement (50x) liquid.

42. Hanna Lab Weizmann Institute of Science. *B27 Supplement (AKA B22)*. vol. 2016 (2016).

43. Garcia-Gonzalo, F. R. & Belmonte, J. C. I. Albumin-associated lipids regulate human embryonic stem cell self-renewal. *PLoS One* **3**, (2008).

44. Longo, N., Frigeni, M. & Pasquali, M. Carnitine transport and fatty acid oxidation. *Biochim. Biophys. Acta - Mol. Cell Res.* **1863**, 2422–2435 (2016).

45. AlbuMAX™ I Lipid-Rich BSA.

46. *AlbuMAX ® I and AlbuMAX ® II*. www.lifetechnologies.com/support.

47. Ludikhuize, M. C., Meerlo, M., Burgering, B. M. T. & Rodríguez Colman, M. J. Protocol to profile the bioenergetics of organoids using Seahorse. *STAR Protoc.* **2**, (2021).

48. Roest, A. S. Vander *et al.* Hypertrophic cardiomyopathy β-cardiac myosin mutation (P710R) leads to hypercontractility by disrupting super relaxed state. *Proc. Natl. Acad. Sci. U. S. A.* **118**, (2021).

49. Mosqueira, D. *et al.* CRISPR/Cas9 editing in human pluripotent stemcell-cardiomyocytes highlights arrhythmias, hypocontractility, and energy depletion as potential therapeutic targets for hypertrophic cardiomyopathy. *Eur. Heart J.* **39**, 3879–3892 (2018).

50. Eschenhagen, T. & Carrier, L. Cardiomyopathy phenotypes in human-induced pluripotent stem cell-derived cardiomyocytes-a systematic review. doi:10.1007/s00424-018-2214-0.

51. Cohn, R. *et al.* A Contraction Stress Model of Hypertrophic Cardiomyopathy due to Sarcomere Mutations. *Stem Cell Reports* **12**, 71–83 (2019).

52. Orosz, A. *et al.* Short-term beat-to-beat variability of the QT interval is increased and correlates with parameters of left ventricular hypertrophy in patients with hypertrophic cardiomyopathy. *Can. J. Physiol. Pharmacol.* **93**, 765–772 (2015).

53. Angelini, A., Pi, X. & Xie, L. Evaluation of long-chain fatty acid respiration in neonatal mouse cardiomyocytes using SeaHorse instrument. *STAR Protoc.* **3**, (2022).

54. Bhagwan, J. R. *et al.* Isogenic models of hypertrophic cardiomyopathy unveil differential phenotypes and mechanism-driven therapeutics. *J. Mol. Cell. Cardiol.* **145**, 43–53 (2020).

55. Mosqueira, Lis-Slimak & Denning. High-Throughput Phenotyping Toolkit for Characterizing

Cellular Models of Hypertrophic Cardiomyopathy in Vitro. *Methods Protoc.* **2**, 83 (2019).

56.	Cortes-Lopez, F. *et al.* Fenofibrate Protects Cardiomyocytes from Hypoxia/Reperfusion- And High Glucose-Induced Detrimental Effects. *PPAR Res.* **2021**, (2021).

57.	Dhahri, W., Couet, J., Roussel, É., Drolet, M. C. & Arsenault, M. Fenofibrate reduces cardiac remodeling and improves cardiac function in a rat model of severe left ventricle volume overload. *Life Sci.* **92**, 26–34 (2013).

58.	Prosdocimo, D. A. *et al.* Kruppel-like factor 15 is a critical regulator of cardiac lipid metabolism. *J. Biol. Chem.* **289**, 5914–5924 (2014).

59.	Knight, W. E. *et al.* Maturation of Pluripotent Stem Cell-Derived Cardiomyocytes Enables Modeling of Human Hypertrophic Cardiomyopathy. *Stem Cell Reports* **16**, 519–533 (2021).

60.	Abdelmagid, S. A. *et al.* Comprehensive profiling of plasma fatty acid concentrations in young healthy canadian adults. *PLoS One* **10**, (2015).

61.	Chun, Y. W. *et al.* Combinatorial polymer matrices enhance in vitro maturation of human induced pluripotent stem cell-derived cardiomyocytes. *Biomaterials* **67**, 52–64 (2015).

62.	Querdel, E. *et al.* Human Engineered Heart Tissue Patches Remuscularize the Injured Heart in a Dose-Dependent Manner. *Circulation* **143**, 1991–2006 (2021).

63.	Murphy, S. A. *et al.* PGC1/PPAR drive cardiomyocyte maturation at single cell level via YAP1 and SF3B2. *Nat. Commun.* **12**, (2021).

7. Supplementary information

Supplementary file 1. Complete list of the used materials and their catalog numbers

Supplementary file 2. Schematic overview of the media formulation

Supplementary file 3-6. Protocols for differentiation, expansion, and maturation of the cell lines (1-6, 1-6-24, 1-16, 1-16-40.5)

Supplementary file 7. IF staining protocol for the 1-6 and 1-6-24 coverslips

This supplementary file contains an extensive table containing all the antibodies used, dilutions, and the incubation times.

Supplementary file 8. Detailed information about the CellProfiler pipeline and laser intensities using the LasX software

Supplementary file 9. Results of the IF test staining for protocol optimization

Supplementary file 10. Protocol of ImageJ quantification of cardiac contraction using the Myocyter plugin

Supplementary file 11. Print screen images for quantification of the areas of the 3D cardiac clusters

In the description of each PowerPoint slide, the area measured with ImageJ is depicted in pixels.

Supplementary file 13. Manufacturer's B27 versus Hanna Lab's B27

Supplementary file 14. Results of Sanger sequencing analysis of the isogenic control cell lines

Supplementary image 1. Raw brightfield image of the 1-6 line shown in Figure 2a
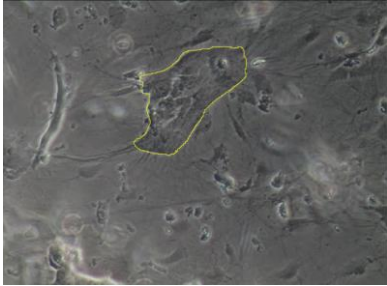
Supplementary image 2. Raw brightfield image of the 1-6-24 line shown in Figure 2a
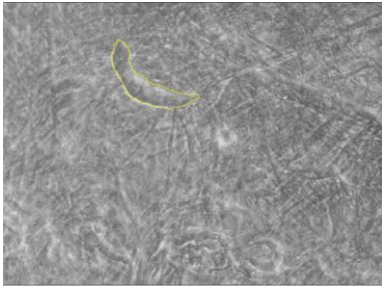
Supplementary image 3. Raw brightfield image of the 1-6 line shown in Figure 7a
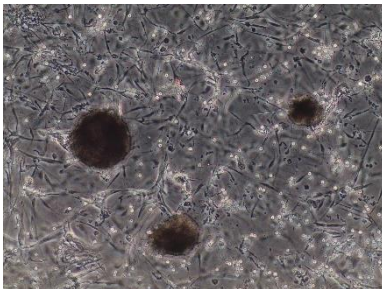
Supplementary image 4. Raw brightfield image of the 1-6-24 line shown in Figure 7a
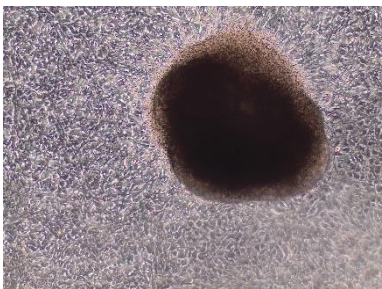
Supplementary image 5. Brightfield image of crystal-like structures in fibrate-treated coverslips
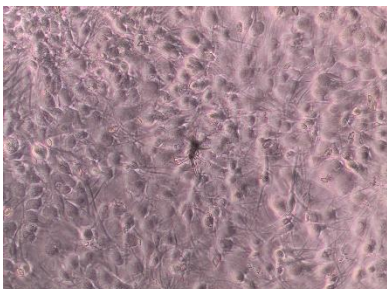
The brightfield image was made at 10x magnification.

Supplementary table 1. Detailed information on the culturing medium components

In this table, the working concentrations of all media components present in the differentiation, thawing, proliferation, replating, and maturation phases are described.

Supplementary table 2. Literature search into fibrate treatments

Supplementary table 3. Raw data from Figure 4b and 4d: Quantification of MYH7 and HADHA staining

Supplementary table 4. Raw data from Figure 4a and 4c: Quantification of ACTN2 and PPARA staining

Supplementary table 5. Raw data from Figure 5: Quantification of CD36 and KLF15 staining

Supplementary table 6. Raw data from Figure 6: OCR and ECAR measurements using seahorse

Supplementary table 7. Raw data from Figure 2 and 3: Cardiac contractility assay quantification

Supplementary table 8. Raw data from Figure 7: Quantification of 3D cardiac clusters

Supplementary video 1. Z-stack video of 1-6 hiPSC-CMs, untreated condition

Supplementary video 2. Z-stack video of 1-6 hiPSC-CMs, fenofibrate-treated condition

Supplementary video 3. Z-stack video of 1-6 hiPSC-CMs, bezafibrate-treated condition

Supplementary video 4. Z-stack video of 1-6-24 hiPSC-CMs, untreated condition

Supplementary video 5. Z-stack video of 1-6-24 hiPSC-CMs, fenofibrate-treated condition

Supplementary video 6. Z-stack video of 1-6-24 hiPSC-CMs, bezafibrate-treated condition

Supplementary video 7. Representative video of the beating 1-6 line prior to fibrate treatment

Supplementary video 8. Representative video of the beating 1-6-24 line prior to fibrate treatment